

1 **A selective LIS1 requirement for mitotic spindle assembly discriminates**
2 **distinct T-cell division mechanisms within the T-cell lineage**

3

4

5 Jérémy Argenty¹, Nelly Rouquié¹, Cyrielle Bories¹, Valérie Duplan¹, Abdelhadi Saoudi¹,
6 Nicolas Fazilleau¹, Renaud Lesourne¹

7

8 ¹ Toulouse Institute for Infectious and Inflammatory Diseases (Infinity), INSERM UMR1291,
9 CNRS UMR5051, University Toulouse III, Toulouse, France.

10

11 Correspondence should be addressed to R.L.

12 Email: renaud.lesourne@inserm.fr

13

14 **Abstract**

15

16 The ability to proliferate is a common feature of most T-cell populations. However,
17 proliferation follows different cell-cycle dynamics and is coupled to different functional
18 outcomes according to T-cell subsets. Whether the mitotic machineries supporting these
19 qualitatively distinct proliferative responses are identical remains unknown. Here, we show that
20 disruption of the microtubule-associated protein LIS1 leads to proliferative defects associated
21 with a blockade of T-cell development after β -selection and of peripheral CD4⁺ T cell
22 expansion after antigen priming. In contrast, cell divisions in CD8⁺ T cells occurred
23 independently of LIS1 following T-cell antigen receptor stimulation, although LIS1 was
24 required for proliferation elicited by pharmacological activation. In thymocytes and CD4⁺ T
25 cells, LIS1-deficiency did not affect signaling events leading to activation but led to an
26 interruption of proliferation after the initial round of division and to p53-induced cell death.
27 Proliferative defects resulted from a mitotic failure, characterized by the presence of extra-
28 centrosomes and the formation of multipolar spindles, causing abnormal chromosomes
29 congression during metaphase and separation during telophase. LIS1 was required to stabilize
30 dynein/dynactin complexes, which promote chromosome attachment to mitotic spindles and
31 ensure centrosome integrity. Together, these results suggest that proliferative responses are
32 supported by distinct mitotic machineries across T-cell subsets.

33

34

35

36

37

38

39 **Introduction**

40

41 Proliferation enables the expansion, differentiation and maintenance of T cells at different
42 stages of their life cycle. It is required for the rapid growth of antigen specific T cells, which is
43 important for efficient control of infection. In this context, the initiation of cell division is
44 primarily driven by signals triggered by the T-cell antigen receptor (TCR), which recognizes
45 self or foreign peptides bound to the major histocompatibility complex (pMHC) at the surface
46 of antigen presenting cells (APCs). Proliferation is also important during T cell development
47 as it enables the expansion of immature CD4-CD8- thymocytes (referred to as double-positive
48 [DN] thymocytes) that have successfully rearranged the TCR β -chain and their differentiation
49 into CD4+CD8+ thymocytes (referred to as double-positive [DP] thymocytes) (1, 2). At these
50 stages, proliferation is mainly driven by coordinated signaling events triggered by the pre-TCR
51 and by the Notch receptor (3, 4). Slow proliferative events are also induced in peripheral T cells
52 to maintain a functional and diversified pool of lymphocytes. Such homeostatic proliferation is
53 triggered in response to TCR stimulation by self-pMHC ligands and to specific cytokines (5).

54

55 CD4+ T helper cells and CD8+ cytotoxic T cells harbor different proliferative characteristics
56 in response to TCR stimulation. CD4+ T cells require repeated TCR stimulation to efficiently
57 divide and show a relatively restricted expansion rate following antigen priming, while CD8+
58 T cells divide rapidly after single TCR stimulation (6, 7). Cell division is associated to the
59 acquisition of effector function in CD8+ T cells (8, 9). The fate decision between the effector
60 and memory lineages in CD8+ T cells has been proposed to occur as early as the first round of
61 division through asymmetric divisions (9), which enables the unequal partitioning of cell fate
62 determinants in daughter cells (8). The role of cell division in the acquisition of CD4+ T cells
63 effector function has been controversial (10, 11). Asymmetric divisions were also reported in

64 CD4⁺ T cells (12, 13), but the contribution of such processes to T helper lineage diversification,
65 which primarily depends on cytokine stimuli, remains also debated (14). Together, these
66 findings suggest that different cell division dynamics and organization might govern
67 proliferation in CD4⁺ and CD8⁺ T cells to ensure different functional outcomes. Whether the
68 mitotic machinery supporting these qualitatively distinct proliferative responses are identical is
69 unknown.

70
71 Lissencephaly gene 1 (LIS1, also known as PAF1B) is a dynein-binding protein which has
72 important function during brain development (15). LIS1 is involved in the proliferation and
73 migration of neural and hematopoietic stem cells (16-18). It binds to the motor protein complex
74 dynein and regulates the dynamic of its interaction with microtubules (15, 19, 20), as well as
75 its ability to form active complex with the multimeric protein complex dynactin (21-23). Those
76 complexes are required for the long transport of cargos toward the minus end of microtubules
77 (24-27) and are important for a wide variety of cellular processes, including the accumulation
78 of γ -tubulin at the centrosome (28, 29) and the efficient formation of mitotic spindle poles
79 during metaphases (30). Recently, we identified LIS1 as a binding partner of the T-cell
80 signaling protein THEMIS (31, 32), which is important for thymocyte positive selection,
81 suggesting that LIS1 could exhibit signaling function during T-cell development. LIS1 is
82 required in several cellular models for chromosome congression and segregation during mitosis
83 and for the establishment of mitotic spindle pole integrity (33). However, the impact of LIS1-
84 deficiency on cell division varies according to cell types and stimulatory contexts. For example,
85 LIS1 is essential to symmetric division of neuroepithelial stem cells prior neurogenesis,
86 whereas LIS1-deficiency has a moderate impact on asymmetric division associated to the
87 differentiation neuroepithelial stem cells in neural progenitors (16). Previous studies also
88 suggest that LIS1 is dispensable for the expansion of CD8⁺ T cells induced following antigen

89 priming (34). Together, these findings suggest that LIS1 could have stage- or subset-specific
90 effects on T-cell mitosis, which might discriminate distinct cellular outcomes.

91

92 Here, we selected LIS1 as a candidate molecule to explore whether T-cell proliferative
93 responses could be supported by distinct mitotic machineries across different T-cell subsets,
94 such as immature thymocytes as well as CD4⁺ and CD8⁺ T cells. Using different *Cre* inducible
95 models, we identified a selective LIS1-requirement for mitosis in thymocytes and peripheral
96 CD4⁺ T cells following β -selection and antigen priming, respectively. In contrast, the
97 disruption of LIS1 had no significant impact on CD8⁺ T cell proliferation mediated by the TCR.
98 In thymocytes and CD4⁺ T cells, LIS1 deficiency led to a disruption of dynein-dynactin
99 complexes, which was associated with a loss of centrosome integrity and with the formation of
100 multipolar spindles. These mitotic abnormalities conducted to abnormal chromosomes
101 congression and separation during metaphase and telophase, and to aneuploidy and p53 up-
102 regulation upon cell division. Together, our results suggest that the mechanisms that support
103 mitosis within the T-cell lineage could vary across T-cell subsets according to the functional
104 outcomes to which they are coupled.

105 **Results**

106

107 **Lis1 deficiency leads to an early block of T- and B-cell development**

108

109 To evaluate the role of LIS1 during T cell development, we conditionally disrupt *Pafah1b1*, the
110 gene encoding LIS1, using a Cre recombinase transgene driven by the human *Cd2*, which is
111 up-regulated in T- and B-cell progenitors (35). Analysis of CD4 and CD8 surface staining in
112 the thymus shows that the loss of LIS1 in the *Cd2-Cre* model leads to a major block of
113 thymocyte maturation at the transition from the DN stage to the DP stage, which is associated
114 with a strong decrease in DP, CD4 and CD8 single-positive [SP] thymocytes numbers but
115 normal numbers of DN thymocytes (Figure 1A). Numbers of peripheral CD4+ and CD8+ T
116 cells were also dramatically decreased in *Cd2-Cre Lis1^{flox/flox}* mice compared to that in control
117 *Lis1^{flox/flox}* mice (Figure 1 – Figure Supplement 1A). Analysis of CD25 and CD44 surface
118 staining on DN thymocytes showed that the numbers of DN4 (CD25-CD44-) thymocytes were
119 strongly decreased in LIS1-deficient mice whereas the numbers of DN3 (CD25+CD44-) and
120 DN2 (CD25+CD44+) thymocytes were increased, pointing-out a defect at the transition from
121 the DN3 to the DN4 stages (Figure 1B). Lower numbers of B cells were also detected in LIS1-
122 deficient mice (Figure 1 – Figure Supplement 1A). Analysis of B cell development in the bone
123 marrow indicates a strong decrease of the numbers of B220+CD19+ pro-B (IgM-c-kit+), pre-
124 B (IgM-c-kit-) and immature B cells (IgM+c-kit-), whereas numbers of pre-pro-B cells
125 (B220+CD19-) were normal, suggesting a defect of maturation of pre-pro-B cells into pro-B
126 cells (Figure 1 – Figure Supplement 1A). Together, these data indicate that LIS1 is essential for
127 early stages of T- and B-cell development.

128

129

130
131
132
133
134
135
136
137
138
139
140
141
142
143
144
145
146
147
148
149
150
151
152
153

LIS1 is required for thymocyte proliferation after the β -selection checkpoint

One critical developmental step at the DN3 to DN4 transition is the formation of a functional TCR β chain, which associates with the pT α chain upon successful rearrangement to form the pre-TCR. Pre-TCR formation triggers signaling events which, together with Notch and the IL-7 receptor (IL-7R) stimulation, lead to the up-regulation of CD5, to the initiation of several division cycles and to further maturation of thymocytes into DN4 thymocytes (1, 2, 4, 36, 37). The percentages of DN3 thymocytes that express the TCR β chain were lower in *Cd2-Cre Lis1^{fllox/fllox}* mice as compared those that in control mice expressing LIS1, suggesting that LIS1 might be important for the rearrangement of the TCR β chain and/or for the expansion of cells that successfully rearranged the TCR β chain (Figure 1C). The expression level of CD5 was slightly increased in *Cd2-Cre Lis1^{fllox/fllox}* DN3 thymocytes compared to that in *Lis1^{fllox/fllox}* DN3 cells, whereas IL-7R cell surface levels was not affected by LIS1 expression, suggesting that LIS1 was not required for functional pre-TCR assembly but rather for the expansion of DN3 thymocytes after the β -selection checkpoint (Figure 1C and 1D). To evaluate whether LIS1 is important for the proliferation of DN3 thymocytes following the β -selection checkpoint, we quantified DN cells that have duplicated DNA copies prior and after the β -selection checkpoint. Thymocytes with duplicated DNA copies could not be detected prior the β -selection checkpoint in wild-type and LIS1-deficient mice (Figure 1E). Approximately 10% of thymocytes were in the G2/M phase of cell cycle after β -selection in wild-type mice whereas this proportion rose to 20% in LIS1-deficient mice, suggesting a possible failure of LIS1-deficient thymocytes to successfully complete division cycles (Figure 1E).

154 To directly address this hypothesis, we analyzed the proliferation of DN3 thymocytes upon
155 stimulation with OP9-D11 cells, a bone-marrow-derived stromal cell line that ectopically
156 expresses the Notch ligand, Delta-like 1 (Dl1), and which induces efficient T-cell
157 lymphopoiesis from the DN stages to the DP stage (38). We observed that the percentages of
158 cells that proliferate in response to OP9-D11 stimulation were strongly decreased in the absence
159 of LIS1 (Figure 2A). This was associated with a failure of DN3 cells to effectively differentiate
160 into CD25-CD44- DN4 cells (Figure 2B). The TCR β chain and the receptor CD5 were up-
161 regulated normally after stimulation, indicating that the defect in proliferation was not the
162 consequence of defects in stimulatory signals required for proliferation and differentiation
163 (Figure 2C). The loss of LIS1 also did not affect the expression of Bcl-2 (Figure 2D), which
164 was shown to be important for efficient survival of DN thymocytes (39, 40), suggesting that
165 the inability of cells to proliferate was not primarily due to survival defects. By contrast, cell
166 cycle analysis showed that the loss of LIS1 led to a strong accumulation of cells at the G2/M
167 stage, indicative of ineffective division processes after the DNA duplication phase (Figure 2E).
168 Together, those results suggest that LIS1 controls cellular events that are required for the
169 efficient division of thymocytes after the β -selection checkpoint.

170

171 **LIS1 is required for TCR-mediated proliferation in CD4⁺ T cells but not in CD8⁺ T cells**

172

173 Previous studies suggested that LIS1-deficient CD4⁺ and CD8⁺ T cells fail to proliferate in
174 response to cytokine-driven homeostatic signals but successfully divide in response to TCR
175 cross-linking *in vitro* or following infection with a *Listeria monocytogenes* strain expressing
176 ovalbumin (34). Since the loss of LIS1 had such a strong impact on thymocyte proliferation
177 following pre-TCR stimulation, we decided to compare the role of LIS1 in the proliferation of
178 CD4⁺ and CD8⁺ T cells in response to TCR engagement.

179

180 To examine the role of LIS1 in peripheral T cells, we conditionally disrupt *Pafah1b1* using a
181 Cre recombinase transgene driven by the *Cd4* promoter, which is up-regulated at the DP stage
182 after the proliferation step of DN3-DN4 thymocytes. We observed that the loss of LIS1 at this
183 stage of development did not affect the percentages and numbers of DN, DP and SP thymocytes
184 (Figure 3 – Figure Supplement 1A). Normal numbers of mature TCR^{hi}CD24^{low} SP thymocytes
185 were also generated in the absence of LIS1 (Figure 3 – Figure Supplement 1B). The maturation
186 of DP thymocytes into TCR^{hi}CD4 SP thymocytes occurred also normally in *Cd4-Cre Lis1^{fllox/fllox}*
187 mice expressing a fixed MHC class II–restricted $\alpha\beta$ -TCR transgene (AND), suggesting that
188 LIS1 is not essential for positive selection (Figure 3 – Figure Supplement 1C). As previously
189 reported in a similar conditional knockout model (34), the deletion of LIS1 led to a dramatic
190 decrease of peripheral CD4⁺ and CD8⁺ T cells numbers (Figure 3 – Figure Supplement 1D).
191 This defect was previously imputed to a reduced ability of CD4⁺ and CD8⁺ T cells to
192 proliferate in response to cytokine-driven homeostatic signals (34).

193

194 We next evaluated the effect of LIS1 deficiency on the proliferation of CD4⁺ and CD8⁺ T cells
195 following TCR stimulation. We observed that the percentages of proliferating CD4⁺ T cells
196 were strongly decreased in the absence of LIS1 following TCR stimulation (Figure 3A). The
197 analysis of percentages of cells in each division cycle showed that LIS1-deficient CD4⁺ T cells
198 successfully performed the first cycle of division but failed to divide further and accumulated
199 at this stage (Figure 3A). Similar results were obtained following stimulation with Phorbol 12-
200 myristate 13-acetate (PMA) and ionomycin, indicating that LIS1-dependent effects on CD4⁺
201 T-cell proliferation were not dependent on proximal TCR signaling events (Figure 3A).
202 Activation markers such as CD25 and CD69 were also up-regulated normally in the absence of
203 LIS1, indicating that more distal TCR signaling events were not affected by LIS1 deficiency

204 (Figure 3B). Cell cycle analysis show that CD4⁺ T cells with duplicated DNA copies
205 accumulated in LIS1-deficient T cells as compared to that in control cells following stimulation
206 (Figure 3C). Contrasting with the strong effect observed on CD4⁺ T cell proliferation, the loss
207 of LIS1 had a rather modest impact on the total fraction of CD8⁺ T cells that proliferate in
208 response to TCR cross-linking and on the fraction of cells that had successfully divided after
209 the first division cycle (Figure 3D). In contrast, the stimulation of CD8⁺ T cells with PMA and
210 ionomycin led to an important decrease of the total fraction of proliferating T cells, suggesting
211 that cell divisions in CD8⁺ T cells are controlled by different mechanisms, which vary
212 according to their LIS1-dependency based on the context of stimulation. To determine whether
213 LIS1 controls the proliferation of CD4⁺ T cells in response to antigen stimulation *in vivo*, we
214 crossed *Cd4-Cre Lis1^{flox/flox}* mice with transgenic mice expressing the allotypic marker CD45.1
215 and the class-II restricted OT2 TCR specific for the chicken ovalbumin 323-339 peptide. CD4⁺
216 T cells from OT2⁺ *Cd4-Cre Lis1^{flox/flox}* and *Lis1^{flox/flox}* mice were stained with CellTrace violet
217 (CTV) and injected into C57Bl/6 mice expressing the allotypic marker CD45.2⁺. Mice were
218 next immunized with ovalbumin and CD45.1⁺CD4⁺ T cells were analyzed in the spleen at day
219 two and three after immunization. The numbers of LIS1-deficient CD45.1⁺ CD4⁺ T cells in
220 the spleen were similar to those of control cells at day two after immunization, indicating that
221 the loss of LIS1 did not affect the ability of CD4⁺ T cells to migrate into the spleen (Figure
222 3E). At this stage, the percentages of divided cells were very low and were not significantly
223 different according to LIS1 expression. At day three after immunization, we observed a large
224 fraction of divided *Lis1^{flox/flox}* CD45.1⁺CD4⁺ T cells, with the majority of cells having
225 completed more than two rounds of division (Figure 3E and 3F). By contrast, the fraction of
226 divided cells was strongly decreased in the absence of LIS1 with almost a complete failure of
227 those cells to engage more than one division cycle (Figure 3E and 3F). Numbers of LIS1-
228 deficient CD4⁺CD45.1⁺ T cells were strongly decreased compared to control CD4⁺CD45.1⁺

229 T cells that express LIS1 (Figure 3E). Of note, the expression level of CD44 on undivided
230 CD4⁺CD45.1⁺ T cells was similar whether or not LIS1 was expressed, suggesting that LIS1
231 was not required for CD4⁺ T-cell activation *in vivo* (Figure 3F). Together, these results suggest
232 that CD4⁺ and CD8⁺ T cells engage distinct cell division mechanisms upon antigen priming
233 that diverge in their requirement for LIS1.

234

235 **LIS1-dependent control of chromosome alignment during metaphase is required for** 236 **effective mitosis**

237

238 We next aimed to more precisely characterize the role of LIS1 during the division of CD4⁺ T
239 cells. Our data suggest a block either at the G2 or the M phase of cell cycle in LIS1-deficient
240 thymocytes and CD4⁺ T cells (Figure 1E, Figure 2E and Figure 3C). We used image stream
241 flow cytometry to discriminate cells with duplicated DNA copies that contain chromosomes (in
242 M phase) from cells that have uncondensed DNA (in G2 phase). *Cd4-Cre Lis1^{flox/flox}* and
243 *Lis1^{flox/flox}* CD4⁺ T cells were stimulated for 48 hours with anti-CD3 and anti-CD28 antibodies
244 and stained with DAPI. Analysis were next performed on cells with duplicated DNA copies.
245 The Bright Detail Intensity (BDI) feature on the DAPI channel, which evaluates areas of peak
246 fluorescence intensity after subtraction of background fluorescence, was selected for its ability
247 to automatically discriminate cells in M and G2 phases, as illustrated in Figure 4A. The
248 percentages of mitotic CD4⁺ T cells were increased in the absence of LIS1, suggesting that
249 LIS1-deficient CD4⁺ T cells fail to achieve mitosis. To determine more precisely the stage of
250 mitosis at which this defect occurs, we analyzed whether LIS1 was required for cells to
251 successfully reach metaphase. *Cd4-Cre Lis1^{flox/flox}* and *Lis1^{flox/flox}* CD4⁺ T cells were stimulated
252 for 48 hours with anti-CD3 and anti-CD28 antibodies and synchronized with nocodazole for 18
253 hours prior treatment with MG132 to induce metaphase arrest. The percentages of cells in

254 metaphase were evaluated by image stream flow cytometry using the “Elongatedness”
255 parameter, which calculates the length to width ratios (L/W) on pre-defined DAPI masks.
256 CD4⁺ T cells with L/W ratios superior to 1.5 show aligned chromosomes patterns
257 representative of metaphase (Figure 4B). This analysis showed that the percentages of cells,
258 which successfully reached metaphase were strongly reduced in the absence of LIS1 (Figure
259 4B). To more precisely characterized mitotic events that could be affected by LIS1-deficiency,
260 we next analyzed the the course of mitosis in *Cd4-Cre Lis1^{flox/flox}* and *Lis1^{flox/flox}* CD4⁺ T cells
261 by time-lapse microscopy. We observed that both *Cd4-Cre Lis1^{flox/flox}* and *Lis1^{flox/flox}* CD4⁺ T
262 cells successfully condensated their DNA to form chromosomes (Figure 4C, video 1 and 2).
263 However, chromosomes remained disorganized in *Cd4-Cre Lis1^{flox/flox}* CD4⁺ T cells and failed
264 to segregate rapidly after condensation as compared to those in control cells (Figure 4C). At the
265 final step of mitosis, LIS1-deficient CD4⁺ T cells either failed to divide (Figure 4C, 4D and
266 video 1) or divided with an apparent unequal repartition of chromosomes in daughter cells
267 (Figure 4C, 4D and video 2), which was associated with the formation of multiple nuclei or
268 multilobed nuclei (Figure 4C and video 2). Confirming the observations based on time-lapse
269 microscopy, quantitative analysis on G2 cells selected by image stream showed that the
270 percentages of cells with multiple nuclei were strongly increased in the absence of LIS1 (Figure
271 4E).

272
273 The abnormal repartition of chromosomes in daughter cells, so called aneuploidy, is generally
274 associated with the up-regulation of the tumor suppressor p53, which contributes to eliminate
275 cells through apoptotic processes prior the emergence of possible oncogenic transformation
276 (41). To determine whether impaired mitosis associated to LIS1-deficiency leads to apoptosis,
277 we analyzed the percentages of apoptotic cells in undivided and divided peripheral CD4⁺ T
278 cells following stimulation with anti-CD3 and anti-CD28 antibodies for 48 hours. We observed

279 that the loss of LIS1 was associated with increased frequency of apoptotic cells among divided
280 cells, but had no significant effect on apoptosis in activated CD25+ undivided cells (Figure
281 5A). Analysis of p53 expression prior the initial cycle of division at 24 hours, showed
282 comparable expression level of p53 between wild-type and LIS1-deficient cells, whereas p53
283 expression was dramatically increased in LIS1-deficient CD4+ T cells as compared to that in
284 control cells after the initial division cycles at 48 hours (Figure 5B). Analysis was next
285 performed on DN3 thymocytes stimulated with OP9-D11 cells and led to a similar increase of
286 apoptosis exclusively in divided thymocytes from LIS1-deficient mice (Figure 5C). The
287 expression level of p53 was also strongly increased in total LIS1-deficient DN3 thymocytes as
288 compared to that in wild-type DN3 cells (Figure 5D). Altogether, those results indicate that the
289 loss of LIS1 results in a defective chromosomes congression and separation during metaphase,
290 which leads to aneuploidy, to the up-regulation of p53 and to the development of apoptotic
291 program.

292

293 **LIS1 controls mitotic spindle and centrosome integrity in CD4+ T cells by promoting the** 294 **formation of dynein-dynactin complexes**

295

296 Each spindle pole is normally established by one centrosome containing a pair of centrioles
297 embedded in the pericentriolar material (PCM) containing γ -tubulin ring complexes (γ -TuRCs)
298 from which microtubules nucleate. Centrosomes replicate once every cell cycle during the G1-
299 S phase (42). Anomaly in centrosomes replication and PCM fragmentation may lead to the
300 formation of extra-centrosomes which can be associated to the formation of multipolar spindles
301 and to the unequal repartition of chromosomes (43, 44). Previous studies in embryonic
302 fibroblast show that the loss of LIS1 is associated with the formation of multipolar spindle due
303 to the formation of extra-centrosomes (33). However, this defect is not systematically observed

304 in the absence of LIS1. For instance, the loss of LIS1 in hematopoietic stem cells has a moderate
305 effect on the integrity of the mitotic spindle but rather affects the spindle positioning during
306 telophase, leading to increased rate of asymmetric divisions (18).

307
308 To evaluate whether the loss of LIS1 could be associated with an aberrant number of
309 centrosomes or to a loss of centrosome integrity prior the division of CD4⁺ T cells, we
310 stimulated CTV stained CD4⁺ T cells from *Cd4-Cre Lis1^{fllox/fllox}* and *Lis1^{fllox/fllox}* mice with anti-
311 CD3 and anti-CD28 antibodies for 48 hours and FACS sorted undivided CTV^{hi} cells based on
312 the forward-size-scattered parameter to discriminate unactivated (forward-scatter [FSC]^{lo}) from
313 activated (FSC^{hi}) cells. Cells were analyzed by confocal microscopy after γ -tubulin and DAPI
314 staining. In the presence of LIS1, we observed that the vast majority of FSC^{lo} CD4⁺ T cells
315 contained a single centrosome, whereas the majority FSC^{hi} cells had two centrosomes as
316 expected from cells in mitosis (Figure 6A). In the absence of LIS1, more than 50% of mitotic
317 FSC^{hi} CD4⁺ T cells had more than two centrosomes (Fig. 6A). The loss of LIS1 did not affect
318 centrosome copy numbers in unactivated CD4⁺ T cells (Figure 6A), indicating that LIS1 is
319 engaged following TCR stimulation once the cell cycle has started, possibly at the stage of
320 centrosome duplication. Some extra-centrosomes showed reduced accumulation of γ -tubulin as
321 compared to normal centrosomes in wild-type cells, suggesting that the loss of LIS1 leads to
322 PCM fragmentation or to the loss of centrosome integrity rather than centrosome
323 supernumerary duplication (Figure 6B). Analysis of γ - and α -tubulin stainings in LIS1-
324 deficient CD4⁺ T cells show that these extra-centrosomes were “active” in that they could
325 effectively nucleate microtubule fibers (Figure 6B). Multiple centrosomes were also observed
326 in cells sorted post- β -selection DN3 thymocytes (Figure 6C). Together, these results indicate
327 that LIS1 is required for the formation of stable bipolar mitotic spindles upon division of
328 thymocytes and CD4⁺ T cells.

329

330 The biochemical basis by which LIS1 affects dynein function has been the focus of intense
331 investigations yielding to contradictory findings and divergent models (15). Evidence from
332 early studies suggest that LIS1 might be acting as a “clutch” that would prevent dynein's
333 ATPase domain from transmitting a detachment signal to its track-binding domain (20). More
334 recent *in vitro* investigations with recombinant proteins identify critical function for LIS1 in
335 the assembly of active dynein-dynactin complexes (21, 22). To analyze whether the cellular
336 defect observed in LIS1-deficient CD4⁺ T cells could be associated with defect in dynein-
337 dynactin complex assembly, we compared the amount of p150Glued, a subunit of the dynactin
338 complex, that co-immunoprecipitated with the intermediate chain of dynein (DIC) in CD4⁺ T
339 cells isolated from *Cd4-Cre Lis1^{flox/flox}* and *Lis1^{flox/flox}* mice (45). The amount of p150Glued that
340 co-immunoprecipitated with DIC was decreased in LIS1-deficient cells as compared to wild-
341 type controls (Figure 6D). Similar amount of the dynein heavy chain (DHC) was co-
342 immunoprecipitated with the DIC in LIS1-deficient and wild-type cells (Figure. 6D), indicating
343 that the defect in DIC-p150Glued interaction was not due do ineffective assembly of the dynein
344 complex itself. These results suggest that LIS1 controls the integrity of mitotic spindle pole
345 assembly in peripheral CD4⁺ T cells by stabilizing the association between dynein and dynactin
346 complexes.

347 **Discussion**

348

349 In this study, we identified a selective LIS1-requirement for mitosis in thymocytes and
350 peripheral CD4⁺ T cells following β -selection and antigen priming, respectively. LIS1-
351 dependent proliferation defects resulted in a block of early T-cell development and in a nearly
352 complete lack of CD4⁺ T-cell expansion following activation. LIS1 deficiency in thymocytes
353 and CD4⁺ T cells led to a disruption of dynein-dynactin complexes, which was associated with
354 a loss of centrosome integrity and with the formation of multipolar spindles. These mitotic
355 abnormalities were in turn associated to abnormal chromosomes reorganization during
356 metaphase and telophase and to aneuploidy and p53 up-regulation upon cell division.
357 Importantly, whereas LIS1 deficiency led to a strong block of CD8⁺ T-cell proliferation upon
358 PMA and ionomycin stimulation, it had very little effects, if any, on the proliferation of CD8⁺
359 T cells following TCR engagement, suggesting that the mitotic machinery that orchestrates
360 mitosis in CD8⁺ T cells upon TCR stimulation is different from that engaged in thymocytes
361 and peripheral CD4⁺ T cells upon pre-TCR and TCR engagement.

362

363 LIS1 was shown to be dispensable for the proliferation of antigen-specific CD8⁺ T cell
364 following infection with *Listeria monocytogenes*, supporting the data that we report here in
365 CD8⁺ T cells following TCR stimulation. Comparable cell type-specific effects of LIS1 on
366 proliferation have been described at early stages of neurogenesis and hematopoiesis (16, 18).
367 The loss of LIS1 in neuroepithelial stem cells leads to mitotic arrest and apoptosis upon
368 symmetrical division events associated to progenitor cell maintenance, whereas it has only a
369 moderate effect on asymmetrical division associated with neurogenesis, suggesting that
370 symmetric division might be more LIS1-sensitive than asymmetric division (16). Accordingly,
371 LIS1-deficiency leads to a dramatic decrease of proliferation when CD8⁺ T cells are stimulated

372 with soluble ligands such as cytokines and PMA/ionomycin, which favor symmetric division
373 (34). This suggests that the different sensitivity of CD4+ and CD8+ T cells to LIS1 deficiency
374 upon cell division is not simply the consequence of a preferential use of LIS1 in CD4+ T cells
375 but rather the consequence of different mitotic organizations in CD4+ and CD8+ T cells in the
376 precise context of polarized cell stimulation, which may exhibit different requirement for LIS1.
377 This raises the question of whether CD4+ T cells would be more prone to symmetric divisions
378 or would engage asymmetric divisions at later stages of expansion than CD8+ T cells. It was
379 suggested that asymmetric divisions occur after several rounds of divisions in CD4+ T cells to
380 enable self-renewal to be coupled to production of differentiated effector CD4+ T cells (13). A
381 possibility is that CD4+ T cells perform preferentially symmetric division, at least during the
382 initial phase of expansion, to maintain an equal level of sensitivity in daughter cells to cytokine-
383 driven signals that primarily determine effector lineage decision in T helper cells. Further
384 experiments would be required to precisely compare qualitative and quantitative aspects of
385 mitosis in CD4+ versus CD8+ T cells in the context of antigen-presenting cell stimulation.

386
387 Mechanistically, we show that LIS1 is important in CD4+ T cells to stabilize the interaction of
388 the microtubule-associated motor protein dynein with the dynactin complex, which facilitates
389 the binding of dynein to cargos and promotes thereby their transport along microtubule fibers.
390 This is in agreement with recent in vitro studies showing that LIS1 is required for the efficient
391 assembly of active dynein-dynactin complexes (21, 22). Given the pleiotropic role of the
392 dynein-dynactin complexes during mitosis, several scenarios could possibly explain the defect
393 of proliferation observed in thymocytes and peripheral CD4+ T cells. Two non-exclusive
394 scenarios seem the most likely to us. A first scenario is that the loss of LIS1 leads to an
395 inefficient attachment of the chromosome kinetochores to dynein, leading to metaphase delay
396 and possibly to the asynchronous chromatid separation, a phenomena call “cohesion fatigue”,

397 which leads to centriole separation and the formation of multipolar spindles (46). This
398 possibility is supported by studies showing that LIS1 is localized to the kinetochores in
399 fibroblasts and is required for the normal alignment of chromosomes during metaphases (33,
400 47) and for targeting the dynein complex to kinetochore (33). A second possibility is that the
401 absence of LIS1 leads to the fragmentation of the PCM, which is associated with the formation
402 of multipolar spindles and the erroneous merotelic kinetochore-microtubule attachments (a
403 single kinetochore attached to microtubules oriented to more than one spindle pole), which can
404 cause chromosomal instability in cells that ultimately undergo bipolar division (48). This is
405 supported by the facts that several PCM components are transported towards centrosomes along
406 microtubules by the dynein–dynactin motor complex (49, 50) and that the depletion of multiple
407 pericentriolar proteins results in PCM fragmentation, which subsequently generates multipolar
408 spindles (50-52).

409
410 We previously identified LIS1 as a binding partner of the signaling protein THEMIS in
411 thymocytes and confirmed this interaction through yeast two-hybrid approaches (31, 32).
412 THEMIS enhances positive selection in thymocytes (53-55) and is important for the
413 maintenance of peripheral CD8⁺ T cells by stimulating cytokine-driven signals leading to
414 homeostatic proliferation (56). Although LIS1 deficiency does not modulate the efficiency of
415 thymocyte positive selection, the loss of LIS1 is associated with a strong defect of peripheral T
416 cell proliferation in response to IL-2 and IL-15 stimulation (34). THEMIS and LIS1
417 deficiencies both lead to severely compromised CD8⁺ T cell proliferation following transfer in
418 lymphopenic hosts (34, 56). Although this defect was attributed to stimulatory function of
419 THEMIS on IL-2 and IL-15-mediated signaling, we cannot rule out the possibility that
420 THEMIS would play a more direct role in cell cycle by controlling LIS1-mediated events.
421 THEMIS operates by repressing the tyrosine phosphatase activity of SHP-1 and SHP-2, which

422 are key regulatory proteins of TCR signaling (57). Gain-of-function mutations of SHP-2 in
423 mouse embryonic fibroblast and leukemia cells lead to centrosome amplification and aberrant
424 mitosis with misaligned chromosomes (58). Thus, the hyper activation of SHP-2 resulting from
425 THEMIS deficiency may lead to cellular defects similar to those observed in LIS1-deficient T
426 cells. An interesting perspective to this work would be to investigate further whether the loss
427 of THEMIS in CD8⁺ T cells would lead to similar mitotic defects to those observed in LIS1-
428 deficient thymocytes and CD4⁺ T cells upon TCR stimulation.

429
430 The fact that LIS1 deficiency increases the frequency of aneuploidy and leads to the up-
431 regulation of p53 expression suggests that defects affecting LIS1 expression or function could
432 favor oncogenic transformation in lymphoid cells. LIS1 is necessary for the extensive growth
433 of tumor cells in some cancer models. The genetic disruption of LIS1 in hematopoietic stem
434 cells blocks the propagation of myeloid leukemia (18). However, several evidences suggest
435 also that the alteration of LIS1 expression could contribute to the carcinogenesis of several
436 cancers such as hepatocellular carcinoma (59, 60), neuroblastoma (61), glioma (62) and
437 cholangiocarcinoma (63). Thus, although a minimal expression level of LIS1 might be
438 mandatory for extensive tumor growth, partial deficiencies in LIS1 might favor oncogenic
439 transformation in a tumor-suppressor failing context. Given the high incidence rates of mitotic
440 defects observed in LIS1 deficient T cells, it is possible that mono-allelic dysfunctions of LIS1
441 might be sufficient to modulate the susceptibility to oncogenic transformation. This could be
442 relevant in humans since genetic variants on *pafah1b1* have been associated with a higher risk
443 to develop acute myeloid leukemia (64).

444

445

446 **Materials and methods**

447 **Mice**

448 *Lis1^{flox/flox}* mice were described previously (65). These mice were bred with hCD2-cre
449 transgenic mice (<https://www.jax.org/strain/008520>) in which the human *cd2* promoter directs
450 the expression of the CRE recombinase at early stages of T and B cell development. *Lis1^{flox/flox}*
451 mice were also bred with CD4-Cre transgenic mice (<https://www.jax.org/strain/017336>) in
452 which the *cd4* promoter directs the expression of the CRE recombinase during T cell
453 development in CD4+CD8+ thymocytes. AND and OT-2 TCR-transgenic mice were from
454 Taconic Farms. All the experiments were conducted with sex and age-matched mice between
455 6 and 12 weeks old housed under specific pathogen-free conditions at the INSERM animal
456 facility (US-006; accreditation number A-31 55508 delivered by the French Ministry of
457 Agriculture to perform experiments on live mice). All experimental protocols were approved
458 by a Ministry-approved ethics committee (CEEA-122) and follow the French and European
459 regulations on care and protection of the Laboratory Animals (EC Directive 2010/63).

460

461 **Antibodies**

462 The following antibodies were used.

463 *For stimulation and cell culture:* anti-CD3 ϵ (145-2C11) and anti-CD28 (37.51) antibodies were
464 from Biolegend. *For cell sorting and flow cytometry analysis:* anti-CD8 α (clone 53-6.7), anti-
465 CD4 (clone RM4-5), anti-CD24 (clone M1/69), anti-TCR β (clone H57-597), anti-V α 11 (clone
466 RR8-1), anti-CD5 (clone 53-7.3), anti-CD69 (clone H1.2F3), anti-B220 (clone RA3-6B2), anti-
467 Gr1 (clone RB6-8C5), anti-CD11b (clone M1/70), anti-CD11c (clone N418), anti-Ter119
468 (clone TER119), anti-CD3 (clone 145-2C11), anti-NK1.1 (clone PK136), anti-TCR $\gamma\delta$ (clone

469 GL3), anti-CD44 (clone IM7), anti-CD25 (clone PC61.5), anti-CD71 (clone R17217), anti-IL-
470 7R (clone A7R34), anti-BCL-2 (clone 3F11), anti-CD19 (clone 1D3/CD19), anti-c-kit (clone
471 2B8), anti-IgM (clone RMM-1) and anti-CD45.1 (clone A20) were from BD Bioscience and
472 Biologend. *For imaging studies:* anti- γ -tubulin (clone 14C11) was from Biologend and anti- α -
473 tubulin (DM1A) was from (Thermo Fisher Scientific). *For immunoprecipitation and Western*
474 *blot analysis:* anti-DIC (clone 74-1), IgG2b isotype control (sc-3879), anti-LIS1 (sc-15319),
475 anti-DHC (sc-9115) were from Santa-Cruz biotechnologies. Anti-p150glued (clone
476 1/p150Glued) were from BD Biosciences, anti-p53 (clone 1C12) were from Cell Signaling and
477 anti-Rac1 (clone 23A8) were from Millipore.

478

479 **Flow cytometry and cell sorting**

480 For flow cytometry analysis, single-cell suspensions from thymus, spleen, lymph nodes and
481 bone marrows were incubated with diluted eBioscience™ Fixable Viability Dye eFluor™ 780
482 (ThermoFisher) in phosphate-buffered saline (PBS) prior staining with fluorochrome-
483 conjugated antibodies. Intracellular staining was performed after cell fixation with 4% para-
484 formaldehyde (PFA) by incubating the cells with conjugated antibodies in permeabilization
485 buffer (Thermo Fisher Scientific). For the phenotyping of DN subsets, thymocytes were stained
486 with an anti-lineage cocktail (anti-Gr1, anti-CD11b, anti-CD11c, anti-Ter119, anti-CD3, anti-
487 B220, anti-NK1.1 and anti-TCR $\gamma\delta$) and with anti-CD8 α and anti-CD4 antibodies. Data
488 acquisition was performed on a BD LSRII flow cytometer and analysis with the FlowJo
489 software.

490 For DN3 cell purification, thymocytes were first immunomagnetically depleted of CD3, CD4
491 or CD8 α positive cells. Lin⁻CD44⁻CD25⁺CD5⁻ or Lin⁻CD44⁻CD25⁺CD71⁻ DN3 cells were
492 sorted on a BD FACS Aria cell sorter. For peripheral T cells isolation, total CD4⁺ T cells and

493 CD8⁺ T cells were purified from ACK-treated pooled lymph nodes and spleen by magnetic
494 immunodepletion of CD8⁺, B220⁺, MHCII⁺, NK1.1⁺, Fcγ⁺ and CD11b⁺ cells and CD4⁺, B220⁺,
495 MHCII⁺, NK1.1⁺, Fcγ⁺ and CD11b⁺ cells, respectively.

496

497 **Cell culture**

498 For OP9-DL1 cells co-cultures, OP9-DL1 cells (38) were seeded at 8000 cells per well in 48-
499 well plates and incubated for 24 hours in OP9 culture media (alpha-MEM, 20% FCS, Penicillin
500 and Streptomycin), followed by addition of 100,000 sorted CD5⁻ or CD71⁻ DN3 thymocytes
501 per well together with 10 ng/ml recombinant mouse IL-7 (PeproTech).

502 For proliferation analysis, CD5⁻ DN3 thymocytes, CD4⁺ and CD8⁺ lymph nodes T cells were
503 labeled with 2 μM CTV (Thermo Fisher Scientific) for 15 min at 37 °C. Thymocytes were
504 cultured with OP9-DL1 cells and peripheral T cells were incubated with the indicated doses of
505 anti-CD3 antibodies and with 2μg/ml anti-CD28 antibodies for 48 and 72 hours. For apoptosis
506 analysis, thymocytes and CD4⁺ T cells were stained with CTV and stimulated for 48 hours as
507 described for proliferation analysis. After stimulation, cells were stained with fluorochrome-
508 conjugated annexin-5 (BD Biosciences) in annexin-5 binding buffer (BD Biosciences). For cell
509 cycle analysis, thymocytes and CD4⁺ T cells were stimulated for 48 hours as indicated above.
510 Cells were fixed with 4% para-formaldehyde (PFA) and incubated with permeabilization buffer
511 prior staining with DAPI in PBS.

512

513

514 **Image stream flow cytometry**

515 For the analysis of the G2/M population, CD4⁺ T cells were stimulated with 10µg/ml of anti-
516 CD3 antibodies with 2µg/ml of anti-CD28 antibodies for 24 hours. Cells were synchronized by
517 addition of nocodazole (Sigma Aldrich) at 100ng/ml for 18h. Cells were then washed in RPMI
518 supplemented with 10% FCS and incubated with 10 µM of MG132 (Sigma Aldrich Cat) for 3h.
519 Cells were incubated with Fixable Viability Dye prior staining with fluochrome-conjugated
520 anti-CD4 antibodies and DAPI and acquired on an ImageStreamX apparatus from Millipore.

521 Data were analyzed using the IDEAS analysis software from Millipore. We used the “Bright
522 Detail Intensity” (BDI) parameter to discriminate mitotic cells from cells in the G2 phase. This
523 parameter calculates the intensity of the bright pixels after subtraction of the background noise
524 from the images. Cells in mitosis having condensed DNA will present a homogeneously bright
525 staining leading to higher BDI value than cells in the G2 phase with uncondensed DNA. To
526 evaluate cells in metaphase, we used the parameter “Elongatedness” which calculates the length
527 to width ratio on a predefined DAPI mask. Cells with an “Elongatedness” value exceeding 1.5
528 were characterized as cells in metaphase.

529

530 **Immunization with ovalbumin**

531 CD45.1⁺ CD4⁺ T cells were purified from lymph nodes and splenocytes from *Lis1^{fllox/fllox}* and
532 *CD4-Cre Lis1^{fllox/fllox}* mice expressing the OT2 TCR. 2x10⁶ cells in PBS were injected i.v. into
533 C57BL/6J mice (CD45.2⁺) one hour before immunization with 40 µg of ovalbumin emulsified
534 with RIBI (Sigma Adjuvant System). CD4⁺ T cell populations from the draining lymph nodes
535 were analyzed 2 and 3 days after immunization.

536 **Confocal analysis**

537 CD4⁺ T cells were labeled with CTV and incubated with 10 µg/ml of anti-CD3 antibodies and
538 2µg/ml of anti-CD28 antibodies for 48 hours. The CTV^{hi}FSC^{lo} (non-proliferating, non-
539 activated) and CTV^{hi}FSC^{hi} (non-proliferating, activated) populations were sorted by flow
540 cytometry. Lin⁻CD44⁺CD25⁺CD5^{hi} thymocytes were sorted by flow cytometry. Cells were
541 deposited on 0.01% poly-L-lysine adsorbed slides (Sigma aldrich), fixed with 4% PFA and
542 permeabilized in PBS containing 0.1% Saponin (Sigma Aldrich). α- and γ-tubulin staining was
543 made in PBS containing 0.1% Saponin, 3% Bovin serum albumin (BSA) and 10mM HEPES at
544 4°C for 18h and revealed with fluorochrome-conjugated anti-mouse and IgG1 and IgG2b
545 antibodies (Thermo Fisher Scientific) for 1 hour at room temperature. DNA was stained with
546 DAPI for 15 min at room temperature in PBS. The slides were then mounted with DABCO
547 solution (Sigma Aldrich) and the images were acquired with an LSM710 confocal microscope
548 equipped with a 63× 1.4 NA objective (Zeiss).

549 For video microscopy, CD4⁺ T cells were cultured with 10 µg/ml of anti-CD3 and 2 µg/ml of
550 anti-CD28 antibodies on a chambered glass coverslip (IBIDI) for 24 hours. To stain DNA,
551 Hoechst 33342 (Sigma-Aldrich) was added to the culture at a final concentration of 50ng/ml.
552 Cells were observed for 18 hours in a chamber at 37°C and 5% CO₂ with a Spinning disk
553 confocal microscope. The z-stack images were edited into film and analyzed using ImageJ.

554 **Immunoprecipitation and Western blot analysis**

555 For immunoprecipitation, CD4⁺ T cells were resuspended in 2 ml of ice-cold lysis buffer (10
556 mM tris-HCl pH 7.4, 150 mM NaCl, 1% Triton, 2 mM Na₃VO₄, 5 mM NaF, 1 mM EDTA, and
557 protease inhibitor cocktail tablet (Roche)) and incubated for 20 min on ice. Lysates were cleared
558 by centrifugation at 18,000g for 15 min at 4°C, and the dynein intermediate chain (DIC) was

559 subjected to immunoprecipitation from cleared lysates for 2 hours at 4°C with 15 µl of protein
560 G-Sepharose resin coated with 12 µg of polyclonal rabbit anti-DIC antibodies. The resin was
561 washed three times and incubated for 10 min at 95°C with Laemmli buffer. For p53 analysis,
562 CD4+ T cells were stimulated with 10 µg/ml of anti-CD3 and 2 µg/ml of anti-CD28 antibodies
563 for 24 and 48 hours and were suspended in ice-cold lysis buffer after each time point.

564
565 Proteins were resolved by SDS-PAGE and transferred to PVDF membranes according to
566 standard protocols. Membranes were blocked with 5% milk in tris-buffered saline containing
567 Tween at 0.05% for 1 hour at room temperature before being incubated with primary antibodies
568 at 4°C overnight. After washing, membranes were incubated with secondary antibodies for 1
569 hour at room temperature. Subsequently, membranes were incubated with enhanced
570 chemiluminescence solution (Sigma) for 5 min in the dark, and luminescence was captured
571 with a Bio-Rad XRS+ imager.

572

573 **Statistical analysis**

574 GraphPad Prism was used to perform statistical analysis. All values in the paper are
575 presented as mean ± SD. Except when indicated, statistical significance was calculated
576 by unpaired two-tailed Mann-Whitney *t* test. **p*<0,05 ***p*<0,001 ****p*<0,0001 *****P* <
577 0.0001.

578

579

580

581 **Data availability**

582

583 All data generated or analyzed during this study are included in the manuscript and supporting

584 files. Source data files have been provided for Figures 1, 2, 3, 4, 5, and 6 as well as for Figure

585 1 – Figure supplement 1 and Figure 3 – Figure supplement 1.

586 **Aknowledgments**

587

588 The authors thank Loïc Dupré for helpful comments and suggestions. We acknowledge the
589 technical assistance provided by the personnel of INSERM US006 Anexplo/creffre animal
590 facility. The authors thank Fatima-Ezzahra L’Faqihi-Olive and Anne-Laure Iscache from the
591 cytometry facility of INFINITy as well as Sophie Allart and Astrid Canivet from the cell
592 imaging facility of INFINITy. Funding: This work was supported by INSERM; the Foundation
593 ARSEP; the Association pour la Recherche sur le Cancer (ARC); the Agence Nationale de la
594 Recherche (ANR-20-CE15-0002); the French Ministry of Higher Education and Research (PhD
595 fellowship for J.A.). Competing interests: The authors declare that they have no competing
596 interests. Data and materials availability: All data needed to evaluate the conclusions of the
597 paper are present in the paper or the Supplementary Materials.

598 **Figure and video legends**

599

600 **Figure 1. LIS1 is required for T cell development following the β -selection checkpoint.**

601 Phenotypic analyses of thymocytes from *Lis^{flox/flox}* and *CD2-Cre Lis^{flox/flox}* mice. (A) Dot plots

602 show CD4 versus CD8 surface staining on thymocytes from *Lis^{flox/flox}* and *CD2-Cre Lis^{flox/flox}*

603 mice. Histogram bars represent the numbers of thymocytes in each indicated subset from mice

604 of the indicated genotype. Data are mean \pm S.D. and represent a pool of four independent

605 experiments each including n=3-4 mice per group. (B) Dot plots show CD44 versus CD25

606 surface staining on CD4-CD8- [DN] thymocytes from *Lis^{flox/flox}* and *CD2-Cre Lis^{flox/flox}* mice.

607 Histogram bars represent the numbers of thymocytes in each indicated subset from mice of the

608 indicated genotype. Data are mean \pm S.D. and represent a pool of five independent experiments

609 each including n=4-5 mice per group. (C) Dot plots show CD5 versus TCR β intracellular

610 staining on DN3 thymocytes from *Lis^{flox/flox}* and *CD2-Cre Lis^{flox/flox}* mice. Histogram bars

611 represent the percentages of TCR β^{hi} CD5 $^{\text{hi}}$ thymocytes in DN3 thymocytes and the MFI of

612 TCR β and CD5 in DN3 TCR β^{hi} CD5 $^{\text{hi}}$ thymocytes from mice of the indicated genotype. Data

613 are mean \pm S.D. and represent a pool of two independent experiments each including n=3 mice

614 per group. (D) Histogram graphs show IL-7R surface staining on DN3 thymocytes from the

615 indicated subsets. Histogram bars represent the MFI of IL-7R in the indicated DN3 thymocytes

616 subsets. Data are mean \pm S.D. and represent a pool of two independent experiments each

617 including n=3 mice per group. (E) Histogram graphs show DNA intracellular staining on DN3

618 thymocytes from the indicated subsets. The percentages represent cells in the G2/M phase of

619 cell cycle. Histogram bars represent the percentages of DN3 TCR β^{hi} CD5 $^{\text{hi}}$ thymocytes in the

620 G2/M phase of cell cycle. Data are mean \pm S.D. and represent a pool of three independent

621 experiments each including n=1 mouse per group. Unpaired two-tailed Mann–Whitney t tests

622 were performed for all analysis. **P < 0.01; ***P < 0.001; ****P < 0.0001.

623

624 **Figure 2. LIS1 is required for the proliferation of immature thymocytes after the β -**

625 **selection checkpoint.** (A) CD5^{lo} DN3 thymocytes from *Lis1^{flox/flox}* and *CD2-Cre Lis1^{flox/flox}* were

626 stained with CTV and stimulated with OP9-D11 cells for 48 or 72 hours. The histogram graph

627 shows CTV dilution. Bar graphs represent the proliferation of cells determined by flow

628 cytometry at 24, 48 and 72 hours after stimulation. Data are mean \pm S.D. and represent three to

629 seven independent experiments each including n=1-2 pooled mice per group. (B) CD5^{lo} DN3

630 thymocytes from *Lis1^{flox/flox}* and *CD2-Cre Lis1^{flox/flox}* were stimulated with OP9-D11 cells for the

631 indicated periods of time. Dot plots show CD44 versus CD25 surface staining on thymocytes

632 from *Lis1^{flox/flox}* and *CD2-Cre Lis1^{flox/flox}* mice. Data are representative of three independent

633 experiments each including n=1-2 pooled mouse per group. (C) CD71^{lo} DN3 thymocytes from

634 *Lis1^{flox/flox}* and *CD2-Cre Lis1^{flox/flox}* were stimulated with OP9-D11 cells for 24 hours. Dot plots

635 show CD5 versus TCR β intracellular staining on thymocytes. Histogram bars represent the

636 percentages of TCR β ^{hi}CD5^{hi} thymocytes in DN3 thymocytes and the MFI of TCR β and CD5

637 in DN3 TCR β ^{hi}CD5^{hi} thymocytes from mice of the indicated genotype. Data are mean \pm S.D.

638 and represent four independent experiments each including n=1-2 pooled mice per group. (D)

639 CD71^{lo} DN3 thymocytes from *Lis1^{flox/flox}* and *CD2-Cre Lis1^{flox/flox}* were stimulated with OP9-

640 D11 cells for 24 hours. The histogram graph shows BCL-2 intracytoplasmic staining in

641 TCR β ^{lo}CD5^{lo} and TCR β ^{hi}CD5^{hi} thymocyte subsets. Histogram bars represent the MFI of BCL-

642 2 in the indicated DN3 thymocyte subsets. Data are mean \pm S.D. and represent three

643 independent experiments each including n=1-2 pooled mice per group. (E) CD71^{lo} DN3

644 thymocytes from *Lis1^{flox/flox}* and *CD2-Cre Lis1^{flox/flox}* were stimulated with OP9-D11 cells for 48

645 hours. Histogram graphs show DNA intracellular staining on thymocytes from the indicated

646 DN3 subsets. The indicated percentages represent cells in the G2/M phase of cell cycle.

647 Histogram bars represent the percentages of DN3 TCR β ^{hi}CD5^{hi} thymocytes in the G2/M phase

648 of cell cycle. Data are mean \pm S.D. and represent six independent experiments each including
649 n=1-2 pooled mice per group. (A) Unpaired two-tailed Welch t tests were performed. (C-E)
650 Unpaired two-tailed Mann–Whitney t tests were performed. *P < 0.05, **P < 0.01.

651

652 **Figure 3. LIS1 is required for the proliferation of CD4⁺ T cells in response to antigen**

653 **stimulation.** (A) CD4⁺ T cells from *Lis1^{flox/flox}* and *CD4-Cre Lis1^{flox/flox}* were stained with CTV

654 and stimulated with anti-CD3 and anti-CD28 antibodies or with PMA and ionomycin (P/I) for

655 72 hours. The histogram graphs show CTV dilution. Bar graphs represent the percentages of

656 cells that divided at least one-time (Tot.) or that divided 1, 2 or 3 times (D1, D2, D3) as

657 determined by flow cytometry at 72 hours after stimulation. Data are mean \pm S.D. and represent

658 five independent experiments each including n=3 mice per group. (B) CD4⁺ T cells from

659 *Lis1^{flox/flox}* and *CD4-Cre Lis1^{flox/flox}* were stimulated with anti-CD3 and anti-CD28 antibodies 24

660 hours. Bar graphs represent the percentages of cells expressing CD25 and CD69 as determined

661 by flow cytometry. Data are mean \pm S.D. and represent two independent experiments each

662 including n=1-2 mice per group. (C) CD4⁺ T cells from *Lis1^{flox/flox}* and *CD4-Cre Lis1^{flox/flox}* were

663 stimulated with anti-CD3 and anti-CD28 antibodies for 48 hours. Histogram graphs show DNA

664 intracellular staining on CD4⁺ T cells. The indicated percentages represent cells in the G2/M

665 phase of cell cycle. Histogram bars represent the percentages of CD4⁺ T cells in the G2/M

666 phase of cell cycle. Data are mean \pm S.D. and represent two independent experiments each

667 including n=3 mice per group. (D) CD8⁺ T cells from *Lis1^{flox/flox}* and *CD4-Cre Lis1^{flox/flox}* were

668 stained with CTV and stimulated with anti-CD3 and anti-CD28 antibodies or with PMA and

669 ionomycin (P/I) for 72 hours. The histogram graph shows CTV dilution. Bar graphs represent

670 the percentages of cells that divided at least one-time (Tot.) or that divided 1, 2 or 3 times (D1,

671 D2, D3) as determined by flow cytometry at 72 hours after stimulation. (E and F) C57BL/6j

672 mice (CD45.2⁺) were injected i.v. with CTV stained CD45.1⁺CD4⁺ T cells from *OT2-Lis1^{flox/flox}*

673 and *OT2-CD4-Cre Lis1^{fllox/fllox}* mice. Mice were then immunized with ovalbumine emulsified in
674 CFA. Proliferation of CD45.1+CD4+ T cells was analyzed at day two and three after
675 immunization. (E) Bar graphs represent the proliferation and numbers of CD45.1+CD4+ T cells
676 as determined by flow cytometry at day two and three after immunization. Data are mean \pm
677 S.D. and are representative of one experiment out of two independent experiments each
678 including n=5 mice per group. (F) The histogram graph shows CTV dilution in CD45.1+CD4+
679 T cells at day 3 after immunization. Histograms overlay shows CD44 surface staining on
680 undivided CD45.1+CD4+ T cells at day 3 after immunization. Data are representative of one
681 experiment out of two independent experiments each including n=5 mice per group. Unpaired
682 two-tailed Mann–Whitney t tests were performed for all analysis. *P < 0.05; **P < 0.01; ***P
683 < 0.001; ****P < 0.0001.

684

685 **Figure 4. Dysfunctional chromosome alignment in LIS1-deficient CD4+ T cells leads to**
686 **abortive mitosis and aneuploidy.** (A) CD4+ T cells from *Lis1^{fllox/fllox}* and *CD4-Cre Lis1^{fllox/fllox}*
687 mice were stimulated with anti-CD3 and anti-CD28 antibodies for 48 hours. Histogram graphs
688 represent the *Bright Detail Intensity* (BDI) feature on CD4+ T cells in the G2/M phase as
689 determined by image stream flow cytometry. Numbers represent the percentages of cells in
690 mitosis according to the BDI feature. Images represent DAPI staining in BDI^{low} and BDI^{hi}
691 *Lis1^{fllox/fllox}* CD4+ T cells. Bar graphs represent the percentages of cells in mitosis (M) out of cells
692 in the G2/M phase. Data are mean \pm S.D. and represent three independent experiments each
693 including n=1 mouse per group. (B) CD4+ T cells from *Lis1^{fllox/fllox}* and *CD4-Cre Lis1^{fllox/fllox}* were
694 stimulated with anti-CD3 and anti-CD28 antibodies for 24 hours, synchronized with
695 nocodazole for 18 hours and incubated with MG132 for 3h to induce metaphase arrest.
696 Histogram graphs represent the *Elongatedness* feature on CD4+ T cells in the M phase as
697 determined by image stream flow cytometry. Numbers represent the percentages of cells in

698 metaphase according to *Elongatedness* feature. Images represent DAPI staining in
699 *Elongatedness*^{low} and *Elongatedness*^{hi} *Lis1*^{flox/flox} CD4⁺ T cells. Bar graphs represent the
700 percentages of cells in metaphase out of cells in the M phase. Data are mean ± S.D. and
701 represent three independent experiments each including n=1 mouse per group. (C) Time-lapse
702 microscopy analysis of cell division in CD4⁺ T cells from *Lis1*^{flox/flox} and *CD4-Cre Lis1*^{flox/flox}
703 stimulated with anti-CD3 and anti-CD28 antibodies. Images represent DNA staining on CD4+
704 T cells at the indicated times (hours:minutes). White arrows represent cells with uncondensed
705 DNA. Red arrows represent the same cells after chromosomes formation. The top red arrows
706 in the *CD4-Cre Lis1*^{flox/flox} panel are representative of abortive mitosis. The bottom red arrows
707 in the *CD4-Cre Lis1*^{flox/flox} panel are representative of mitosis leading to aneuploidy. Bar graphs
708 represent the time of mitosis per cell. Data are mean ± S.D. and represent three independent
709 experiments each including n=1 mouse per group. (D) Mitosis outcomes in *Lis1*^{flox/flox} and *CD4-*
710 *Cre Lis1*^{flox/flox} CD4⁺ T cells stimulated with anti-CD3 and anti-CD28 antibodies. Numbers
711 represent percentages in the different section out of a total of n=62-64 mitosis analyzed. Data
712 represent three independent experiments each including n=1 mouse per group. (E) CD4⁺ T cells
713 from *Lis1*^{flox/flox} and *CD4-Cre Lis1*^{flox/flox} were stimulated with anti-CD3 and anti-CD28
714 antibodies for 48 hours. Cells in G2 phase were analyzed by image stream flow cytometry.
715 Cells stained with DAPI and Bright-field (BF) images are represented. Bar graphs represent the
716 percentages of cells with multilobed nuclei. Data are mean ± S.D. and represent three
717 independent experiments each including n=1 mouse per group. (A and B) Unpaired two-tailed
718 Welch t tests were performed. (C) Unpaired two-tailed Mann–Whitney t test was performed.
719 *P < 0.05; **P < 0.01; ***P < 0.001; ****P < 0.0001.

720

721 **Figure 5. Proliferation leads to p53 up-regulation and apoptosis in LIS1-deficient**
722 **thymocytes and CD4⁺ T cells.** (A) CD4⁺ T cells from *Lis1*^{flox/flox} and *CD4-Cre Lis1*^{flox/flox} were

723 stained with CTV and stimulated with anti-CD3 and anti-CD28 antibodies for 48 hours. The
724 histogram graphs show annexin-5 staining on CTV^{hi} (top panel) and CTV^{low} (bottom panel)
725 CD25⁺CD4⁺ T cells. Bar graphs represent the percentages of annexin5⁺ cells in the indicated
726 subsets. Data are mean \pm S.D. and represent two independent experiments each including n=1-
727 2 mice per group. (B) Total CD4⁺ T cells from *Lis1^{fllox/fllox}* and *CD4-Cre Lis1^{fllox/fllox}* mice were
728 stimulated anti-CD3 and anti-CD28 antibodies for the indicated times. Total cytoplasmic
729 extracts of the cells were then analyzed by Western blotting with antibodies against p53 and
730 Rac1, the loading control. Data are representative of two independent experiments. (C) CD5^{lo}
731 DN3 thymocytes from *Lis1^{fllox/fllox}* and *CD2-Cre Lis1^{fllox/fllox}* were stained with CTV and stimulated
732 with OP9-D11 cells for 48 hours. The histogram graphs show annexin-5 staining on CTV^{hi} (top
733 panel) and CTV^{low} (bottom panel) CD5^{hi}CD4⁺ T cells. Bar graphs represent the percentages of
734 annexin5⁺ cells in the indicated subsets. Data are mean \pm S.D. and represent two independent
735 experiments each including n=2 mice per group. (D) Total cytoplasmic extracts of the DN
736 thymocytes were analyzed by Western blotting with antibodies against p53 and Rac1, the
737 loading control. Data are representative of two independent experiments. Unpaired two-tailed
738 Welch t tests were performed in A and C. *P < 0.05; ***P < 0.001.

739
740 **Figure 6. Impaired formation of dynein/dynactin complexes is associated with the loss of**
741 **centrosome integrity and the formation of multipolar spindles in LIS-1 deficient**
742 **thymocytes and CD4⁺ T cells.** (A) CD4⁺ T cells from *Lis1^{fllox/fllox}* and *CD4-Cre Lis1^{fllox/fllox}* were
743 stained with CTV and stimulated with anti-CD3 and anti-CD28 antibodies for 48 hours. Images
744 represent Maximum Intensity Projection of γ -tubulin and DAPI staining on undivided FSC^{lo}
745 (top panel) and FSC^{hi} (bottom panel) CD4⁺ T cells. Bar graphs represent the percentages of
746 cells with the indicated number of centrosome in total cells (top graph) or in mitotic cells
747 (bottom graph). Data represent one experiment out of two independent experiments with n=30-

748 50 cells analyzed per group. (B) CD4⁺ T cells from *Lis1^{lox/lox}* and *CD4-Cre Lis1^{lox/lox}* mice
749 were stained with CTV and stimulated with anti-CD3 and anti-CD28 antibodies for 48 hours.
750 Images represent Maximum Intensity Projection of γ -tubulin and α -tubulin staining on
751 undivided FSC^{hi} CD4⁺ T cells. Bar graphs represent the size of the pericentriolar region (PCM)
752 based on γ -tubulin staining in mitotic cells with the indicated number of centrosomes. Data
753 represent one experiment out of two independent experiments with n=30-50 cells analyzed per
754 group. (C) Images represent Maximum Intensity Projection of γ -tubulin and DAPI staining
755 CD5^{hi} DN3 thymocytes. Bar graphs represent the percentages of cells with the indicated number
756 of centrosomes in mitotic cells. Data represent one experiment out of two independent
757 experiments with n=30-50 cells analyzed per group. (D) CD4⁺ T cell extracts from *Lis1^{lox/lox}*
758 and *CD4-Cre Lis1^{lox/lox}* mice were subjected to immunoprecipitation (IP) with antibodies
759 specific of the intermediate chain of dynein (DIC) or with an IgG2b isotype control and then
760 analyzed by Western blotting with antibodies specific of the indicated proteins (Dynein heavy
761 chain [DHC]). Data represent one experiment out of two independent experiments. Unpaired
762 two-tailed Mann–Whitney t test was performed. ****P < 0.0001.

763
764 **Video 1. Time-lapse microscopy of abortive mitosis in Lis1-deficient CD4⁺ T cells.** Time-
765 lapse microscopy analysis of mitosis in CD4⁺ T cells from *Lis1^{lox/lox}* mice stimulated with anti-
766 CD3 and anti-CD28 antibodies. Videos represent DNA staining (left panel) and bright field
767 (right panel) on CD4⁺ T cells.

768
769 **Video 2. Time-lapse microscopy of mitosis with aneuploidy in Lis1-deficient CD4⁺ T cells.**
770 Time-lapse microscopy analysis of mitosis in CD4⁺ T cells from *Lis1^{lox/lox}* mice stimulated
771 with anti-CD3 and anti-CD28 antibodies. Videos represent DNA staining (left panel) and bright
772 field (right panel) on CD4⁺ T cells.

773 **Figure S1. LIS1 is required for B cell development.** (A) Dot plots show TCR versus B220
774 and CD4 versus CD8 surface staining on splenocytes from *Lis1^{fllox/fllox}* and *CD2-Cre Lis1^{fllox/fllox}*
775 mice. Histogram bars represent the numbers of thymocytes in each indicated subset from mice
776 of the indicated genotype. Data are mean \pm S.D. and represent four independent experiments
777 each including n=3-4 mice per group. (B) Upper dot plots show B220 versus CD19 on bone
778 marrow cells from *Lis1^{fllox/fllox}* and *CD2-Cre Lis1^{fllox/fllox}* mice. Lower dot plots show IgM versus
779 c-Kit staining on B220⁺CD19⁺ bone marrow cells from *Lis1^{fllox/fllox}* and *CD2-Cre Lis1^{fllox/fllox}* mice.
780 Histogram bars represent the numbers of cells in each indicated subset from mice of the
781 indicated genotype. Data are mean \pm S.D. and represent two independent experiments each
782 including n=3-4 mice per group. Unpaired two-tailed Mann–Whitney t test were performed. *P
783 < 0.05; **P < 0.01; ***P < 0.001; ****P < 0.0001.

784
785 **Figure S2. Normal T cell development in *CD4-Cre Lis1^{fllox/fllox}* mice.** Phenotypic analyses of
786 thymocytes from *Lis1^{fllox/fllox}* and *CD4-Cre Lis1^{fllox/fllox}* mice. (A) Dot plots show CD4 versus CD8
787 surface staining on thymocytes from *Lis1^{fllox/fllox}* and *CD4-Cre Lis1^{fllox/fllox}* mice. Histogram bars
788 represent the numbers of thymocytes in each indicated subset from mice of the indicated
789 genotype. Data are mean \pm S.D. and represent two independent experiments each including
790 n=2-3 mice per group. (B) Dot plots show CD24 versus TCR β surface staining on CD4⁺ SP
791 and CD8⁺ SP thymocytes from *Lis1^{fllox/fllox}* and *CD4-Cre Lis1^{fllox/fllox}* mice. Histogram bars
792 represent the numbers of thymocytes in the indicated subset from mice of the indicated
793 genotype. Data are mean \pm S.D. and represent two independent experiments each including n=2
794 mice per group. (C) Dot plots show CD4 versus CD8 surface staining on thymocytes from
795 *Lis1^{fllox/fllox}* and *CD4-Cre Lis1^{fllox/fllox}* mice expressing the AND TCR transgene. Histogram graphs
796 represent the TCR V α 11 surface staining on total thymocytes. Histogram bars represent the
797 numbers of thymocytes in each indicated subset from mice of the indicated genotype. Data are

798 mean \pm S.D. and represent two independent experiments each including n=2-3 mice per group.

799 (D) Dot plots show TCR versus B220 and CD4 versus CD8 surface staining on splenocytes

800 from *Lis1^{flox/flox}* and *CD4-Cre Lis1^{flox/flox}* mice. Histogram bars represent the numbers of cells in

801 each indicated subset from mice of the indicated genotype. Data are mean \pm S.D. and represent

802 two independent experiments each including n=2-3 mice per group. *P < 0.05; **P < 0.01;

803 ***P < 0.001; ****P < 0.0001.

804

805

806

807 References

808

- 809 1. Kreslavsky T, Gleimer M, Miyazaki M, Choi Y, Gagnon E, Murre C, et al. beta-
810 Selection-induced proliferation is required for alphabeta T cell differentiation. *Immunity*.
811 2012;37(5):840-53.
- 812 2. Penit C, Lucas B, Vasseur F. Cell expansion and growth arrest phases during the
813 transition from precursor (CD4-8-) to immature (CD4+8+) thymocytes in normal and
814 genetically modified mice. *J Immunol*. 1995;154(10):5103-13.
- 815 3. Ciofani M, Schmitt TM, Ciofani A, Michie AM, Cuburu N, Aublin A, et al. Obligatory
816 role for cooperative signaling by pre-TCR and notch during thymocyte differentiation. *Journal*
817 *of Immunology*. 2004;172(9):5230-9.
- 818 4. Maillard I, Tu L, Sambandam A, Yashiro-Ohtani Y, Millholland J, Keeshan K, et al.
819 The requirement for Notch signaling at the beta-selection checkpoint in vivo is absolute and
820 independent of the pre-T cell receptor. *The Journal of experimental medicine*.
821 2006;203(10):2239-45.
- 822 5. Sprent J, Surh CD. Normal T cell homeostasis: the conversion of naive cells into
823 memory-phenotype cells. *Nat Immunol*. 2011;12(6):478-84.
- 824 6. Foulds KE, Zenewicz LA, Shedlock DJ, Jiang J, Troy AE, Shen H. Cutting edge: CD4
825 and CD8 T cells are intrinsically different in their proliferative responses. *Journal of*
826 *Immunology*. 2002;168(4):1528-32.
- 827 7. Seder RA, Ahmed R. Similarities and differences in CD4(+) and CD8(+) effector and
828 memory T cell generation. *Nature immunology*. 2003;4(9):835-42.
- 829 8. Chang JT, Palanivel VR, Kinjyo I, Schambach F, Intlekofer AM, Banerjee A, et al.
830 Asymmetric T lymphocyte division in the initiation of adaptive immune responses. *Science*.
831 2007;315(5819):1687-91.
- 832 9. Arsenio J, Kakaradov B, Metz PJ, Kim SH, Yeo GW, Chang JT. Early specification of
833 CD8(+) T lymphocyte fates during adaptive immunity revealed by single-cell gene-expression
834 analyses. *Nature immunology*. 2014;15(4):365-+.
- 835 10. Bird JJ, Brown DR, Mullen AC, Moskowitz NH, Mahowald MA, Sider JR, et al. Helper
836 T cell differentiation is controlled by the cell cycle. *Immunity*. 1998;9(2):229-37.
- 837 11. Ben-Sasson SZ, Gerstel R, Hu-Li J, Paul WE. Cell division is not a "clock" measuring
838 acquisition of competence to produce IFN-gamma or IL-4. *Journal of Immunology*.
839 2001;166(1):112-20.
- 840 12. Chang JT, Ciocca ML, Kinjyo I, Palanivel VR, McClurkin CE, De Jong CS, et al.
841 Asymmetric Proteasome Segregation as a Mechanism for Unequal Partitioning of the
842 Transcription Factor T-bet during T Lymphocyte Division. *Immunity*. 2011;34(4):492-504.
- 843 13. Nish SA, Zens KD, Kratchmarov R, Lin WHW, Adams WC, Chen YH, et al. CD4(+)
844 T cell effector commitment coupled to self-renewal by asymmetric cell divisions. *Journal of*
845 *Experimental Medicine*. 2017;214(1):39-47.
- 846 14. Cobbold SP, Adams E, Howie D, Waldmann H. CD4(+) T Cell Fate Decisions Are
847 Stochastic, Precede Cell Division, Depend on GITR Co-Stimulation, and Are Associated With
848 Uropodium Development. *Frontiers in immunology*. 2018;9.
- 849 15. Markus SM, Marzo MG, McKenney RJ. New insights into the mechanism of dynein
850 motor regulation by lissencephaly-1. *Elife*. 2020;9.
- 851 16. Yingling J, Youn YH, Darling D, Toyo-Oka K, Pramparo T, Hirotsune S, et al.
852 Neuroepithelial stem cell proliferation requires LIS1 for precise spindle orientation and
853 symmetric division. *Cell*. 2008;132(3):474-86.

- 854 17. Reiner O, Sapir T. LIS1 functions in normal development and disease. *Current opinion*
855 *in neurobiology*. 2013;23(6):951-6.
- 856 18. Zimdahl B, Ito T, Blevins A, Bajaj J, Konuma T, Weeks J, et al. Lis1 regulates
857 asymmetric division in hematopoietic stem cells and in leukemia. *Nature genetics*.
858 2014;46(3):245-+.
- 859 19. Yamada M, Toba S, Yoshida Y, Haratani K, Mori D, Yano Y, et al. LIS1 and NDEL1
860 coordinate the plus-end-directed transport of cytoplasmic dynein. *Embo Journal*.
861 2008;27(19):2471-83.
- 862 20. Huang J, Roberts AJ, Leschziner AE, Reck-Peterson SL. Lis1 Acts as a "Clutch"
863 between the ATPase and Microtubule-Binding Domains of the Dynein Motor. *Cell*.
864 2012;150(5):975-86.
- 865 21. Htet ZM, Gillies JP, Baker RW, Leschziner AE, DeSantis ME, Reck-Peterson SL. LIS1
866 promotes the formation of activated cytoplasmic dynein-1 complexes. *Nature cell biology*.
867 2020;22(5):518-+.
- 868 22. Elshenawy MM, Kusakci E, Volz S, Baumbach J, Bullock SL, Yildiz A. Lis1 activates
869 dynein motility by modulating its pairing with dynactin. *Nature cell biology*. 2020;22(5):570-
870 8.
- 871 23. Wang S, Ketcham SA, Schon A, Goodman B, Wang Y, Yates J, 3rd, et al. Nudel/NudE
872 and Lis1 promote dynein and dynactin interaction in the context of spindle morphogenesis.
873 *Molecular biology of the cell*. 2013;24(22):3522-33.
- 874 24. McKenney RJ, Huynh W, Tanenbaum ME, Bhabha G, Vale RD. Activation of
875 cytoplasmic dynein motility by dynactin-cargo adapter complexes. *Science*.
876 2014;345(6194):337-41.
- 877 25. Ayloo S, Lazarus JE, Dodda A, Tokito M, Ostap EM, Holzbaur EL. Dynactin functions
878 as both a dynamic tether and brake during dynein-driven motility. *Nat Commun*. 2014;5:4807.
- 879 26. Urnavicius L, Zhang K, Diamant AG, Motz C, Schlager MA, Yu M, et al. The structure
880 of the dynactin complex and its interaction with dynein. *Science*. 2015;347(6229):1441-6.
- 881 27. Schlager MA, Hoang HT, Urnavicius L, Bullock SL, Carter AP. In vitro reconstitution
882 of a highly processive recombinant human dynein complex. *EMBO J*. 2014;33(17):1855-68.
- 883 28. Young A, Dichtenberg JB, Purohit A, Tuft R, Doxsey SJ. Cytoplasmic dynein-mediated
884 assembly of pericentrin and gamma tubulin onto centrosomes. *Molecular biology of the cell*.
885 2000;11(6):2047-56.
- 886 29. Blagden SP, Glover DM. Polar expeditions--provisioning the centrosome for mitosis.
887 *Nature cell biology*. 2003;5(6):505-11.
- 888 30. Quintyne NJ, Schroer TA. Distinct cell cycle-dependent roles for dynactin and dynein
889 at centrosomes. *Journal of Cell Biology*. 2002;159(2):245-54.
- 890 31. Zvezdova E, Mikolajczak J, Garreau A, Marcellin M, Rigal L, Lee J, et al. Themis1
891 enhances T cell receptor signaling during thymocyte development by promoting Vav1 activity
892 and Grb2 stability. *Science signaling*. 2016;9(428):ra51.
- 893 32. Garreau A, Blaize G, Argenty J, Rouquie N, Tourdes A, Wood SA, et al. Grb2-Mediated
894 Recruitment of USP9X to LAT Enhances Themis Stability following Thymic Selection. *J*
895 *Immunol*. 2017;199(8):2758-66.
- 896 33. Moon HM, Youn YH, Pemble H, Yingling J, Wittmann T, Wynshaw-Boris A. LIS1
897 controls mitosis and mitotic spindle organization via the LIS1-NDEL1-dynein complex. *Hum*
898 *Mol Genet*. 2014;23(2):449-66.
- 899 34. Ngoi SM, Lopez JM, Chang JT. The Microtubule-Associated Protein Lis1 Regulates T
900 Lymphocyte Homeostasis and Differentiation. *J Immunol*. 2016.
- 901 35. Greaves DR, Wilson FD, Lang G, Kioussis D. Human CD2 3'-flanking sequences confer
902 high-level, T cell-specific, position-independent gene expression in transgenic mice. *Cell*.
903 1989;56(6):979-86.

- 904 36. Boudil A, Matei IR, Shih HY, Bogdanoski G, Yuan JS, Chang SG, et al. IL-7
905 coordinates proliferation, differentiation and TcrA recombination during thymocyte beta-
906 selection. *Nature immunology*. 2015;16(4):397-405.
- 907 37. Azzam HS, Grinberg A, Lui K, Shen H, Shores EW, Love PE. CD5 expression is
908 developmentally regulated by T cell receptor (TCR) signals and TCR avidity. *Journal of*
909 *Experimental Medicine*. 1998;188(12):2301-11.
- 910 38. Schmitt TM, de Pooter RF, Gronski MA, Cho SK, Ohashi PS, Zuniga-Pflucker JC.
911 Induction of T cell development and establishment of T cell competence from embryonic stem
912 cells differentiated in vitro. *Nature immunology*. 2004;5(4):410-7.
- 913 39. Akashi K, Kondo M, von Freeden-Jeffry U, Murray R, Weissman IL. Bcl-2 rescues T
914 lymphopoiesis in interleukin-7 receptor-deficient mice. *Cell*. 1997;89(7):1033-41.
- 915 40. Maraskovsky E, O'Reilly LA, Teepe M, Corcoran LM, Peschon JJ, Strasser A. Bcl-2
916 can rescue T lymphocyte development in interleukin-7 receptor-deficient mice but not in
917 mutant rag-1(-/-) mice. *Cell*. 1997;89(7):1011-9.
- 918 41. Kasthuber ER, Lowe SW. Putting p53 in Context. *Cell*. 2017;170(6):1062-78.
- 919 42. Nigg EA, Stearns T. The centrosome cycle: Centriole biogenesis, duplication and
920 inherent asymmetries. *Nature cell biology*. 2011;13(10):1154-60.
- 921 43. Holland AJ, Cleveland DW. Boveri revisited: chromosomal instability, aneuploidy and
922 tumorigenesis. *Nature reviews Molecular cell biology*. 2009;10(7):478-87.
- 923 44. Maiato H, Logarinho E. Mitotic spindle multipolarity without centrosome amplification.
924 *Nature cell biology*. 2014;16(5):386-U23.
- 925 45. Reck-Peterson SL, Redwine WB, Vale RD, Carter AP. The cytoplasmic dynein
926 transport machinery and its many cargoes (vol 19, pg 382, 2018). *Nat Rev Mol Cell Bio*.
927 2018;19(7):479-.
- 928 46. Daum JR, Potapova TA, Sivakumar S, Daniel JJ, Flynn JN, Rankin S, et al. Cohesion
929 Fatigue Induces Chromatid Separation in Cells Delayed at Metaphase. *Current Biology*.
930 2011;21(12):1018-24.
- 931 47. Faulkner NE, Dujardin DL, Tai CY, Vaughan KT, O'Connell CB, Wangs YL, et al. A
932 role for the lissencephaly gene LIS1 in mitosis and cytoplasmic dynein function. *Nature cell*
933 *biology*. 2000;2(11):784-91.
- 934 48. Cimini D, Howell B, Maddox P, Khodjakov A, Degrossi F, Salmon ED. Merotelic
935 kinetochore orientation is a major mechanism of aneuploidy in mitotic mammalian tissue cells.
936 *Journal of Cell Biology*. 2001;153(3):517-27.
- 937 49. Barenz F, Mayilo D, Gruss OJ. Centriolar satellites: Busy orbits around the centrosome.
938 *European Journal of Cell Biology*. 2011;90(12):983-9.
- 939 50. Dammermann A, Merdes A. Assembly of centrosomal proteins and microtubule
940 organization depends on PCM-1. *Journal of Cell Biology*. 2002;159(2):255-66.
- 941 51. Krauss SW, Spence JR, Bahmanyar S, Barth AIM, Go MM, Czerwinski D, et al.
942 Downregulation of protein 4.1R, a mature centriole protein, disrupts centrosomes, alters cell
943 cycle progression, and perturbs mitotic spindles and anaphase. *Molecular and cellular biology*.
944 2008;28(7):2283-94.
- 945 52. Kim K, Rhee K. The pericentriolar satellite protein CEP90 is crucial for integrity of the
946 mitotic spindle pole. *Journal of cell science*. 2011;124(Pt 3):338-47.
- 947 53. Fu G, Vallee S, Rybakin V, McGuire MV, Ampudia J, Brockmeyer C, et al. Themis
948 controls thymocyte selection through regulation of T cell antigen receptor-mediated signaling.
949 *Nature immunology*. 2009;10(8):848-56.
- 950 54. Lesourne R, Uehara S, Lee J, Song KD, Li L, Pinkhasov J, et al. Themis, a T cell-
951 specific protein important for late thymocyte development. *Nature immunology*.
952 2009;10(8):840-7.

- 953 55. Johnson AL, Aravind L, Shulzhenko N, Morgun A, Choi SY, Crockford TL, et al.
954 Themis is a member of a new metazoan gene family and is required for the completion of
955 thymocyte positive selection. *Nature immunology*. 2009;10(8):831-9.
- 956 56. Brzostek J, Gautam N, Zhao X, Chen EW, Mehta M, Tung DWH, et al. T cell receptor
957 and cytokine signal integration in CD8(+) T cells is mediated by the protein Themis. *Nature*
958 *immunology*. 2020;21(2):186-+.
- 959 57. Choi S, Warzecha C, Zvezdova E, Lee J, Argenty J, Lesourne R, et al. THEMIS
960 enhances TCR signaling and enables positive selection by selective inhibition of the
961 phosphatase SHP-1. *Nature immunology*. 2017.
- 962 58. Liu X, Zheng H, Li X, Wang S, Meyerson HJ, Yang W, et al. Gain-of-function
963 mutations of Ptpn11 (Shp2) cause aberrant mitosis and increase susceptibility to DNA damage-
964 induced malignancies. *Proceedings of the National Academy of Sciences of the United States*
965 *of America*. 2016;113(4):984-9.
- 966 59. Li XL, Liu LS, Li R, Wu AL, Lu JQ, Wu QZ, et al. Hepatic loss of Lissencephaly 1
967 (Lis1) induces fatty liver and accelerates liver tumorigenesis in mice. *Journal of Biological*
968 *Chemistry*. 2018;293(14):5160-71.
- 969 60. Xing Z, Tang X, Gao Y, Da L, Song H, Wang SQ, et al. The human LIS1 is
970 downregulated in hepatocellular carcinoma and plays a tumor suppressor function. *Biochem*
971 *Bioph Res Co*. 2011;409(2):193-9.
- 972 61. Messi E, Florian MC, Caccia C, Zanisi M, Maggi R. Retinoic acid reduces human
973 neuroblastoma cell migration and invasiveness: effects on DCX, LIS1, neurofilaments-68 and
974 vimentin expression. *Bmc Cancer*. 2008;8.
- 975 62. Suzuki SO, McKenney RJ, Mawatari S, Mizuguchi M, Mikami A, Iwaki T, et al.
976 Expression patterns of LIS1, dynein and their interaction partners dynactin, NudE, NudEL and
977 NudC in human gliomas suggest roles in invasion and proliferation. *Acta Neuropathol*.
978 2007;113(5):591-9.
- 979 63. Yang R, Chen YJ, Tang C, Li HB, Wang B, Yan Q, et al. MicroRNA-144 suppresses
980 cholangiocarcinoma cell proliferation and invasion through targeting platelet activating factor
981 acetylhydrolase isoform 1b. *Bmc Cancer*. 2014;14.
- 982 64. Cao SY, Lu XM, Wang LH, Qian XF, Jin GF, Ma HX. The functional polymorphisms
983 of LIS1 are associated with acute myeloid leukemia risk in a Han Chinese population. *Leukemia*
984 *Res*. 2017;54:7-11.
- 985 65. Hirotsume S, Fleck MW, Gambello MJ, Bix GJ, Chen A, Clark GD, et al. Graded
986 reduction of Pafah1b1 (Lis1) activity results in neuronal migration defects and early embryonic
987 lethality. *Nature genetics*. 1998;19(4):333-9.
- 988

Figure 1

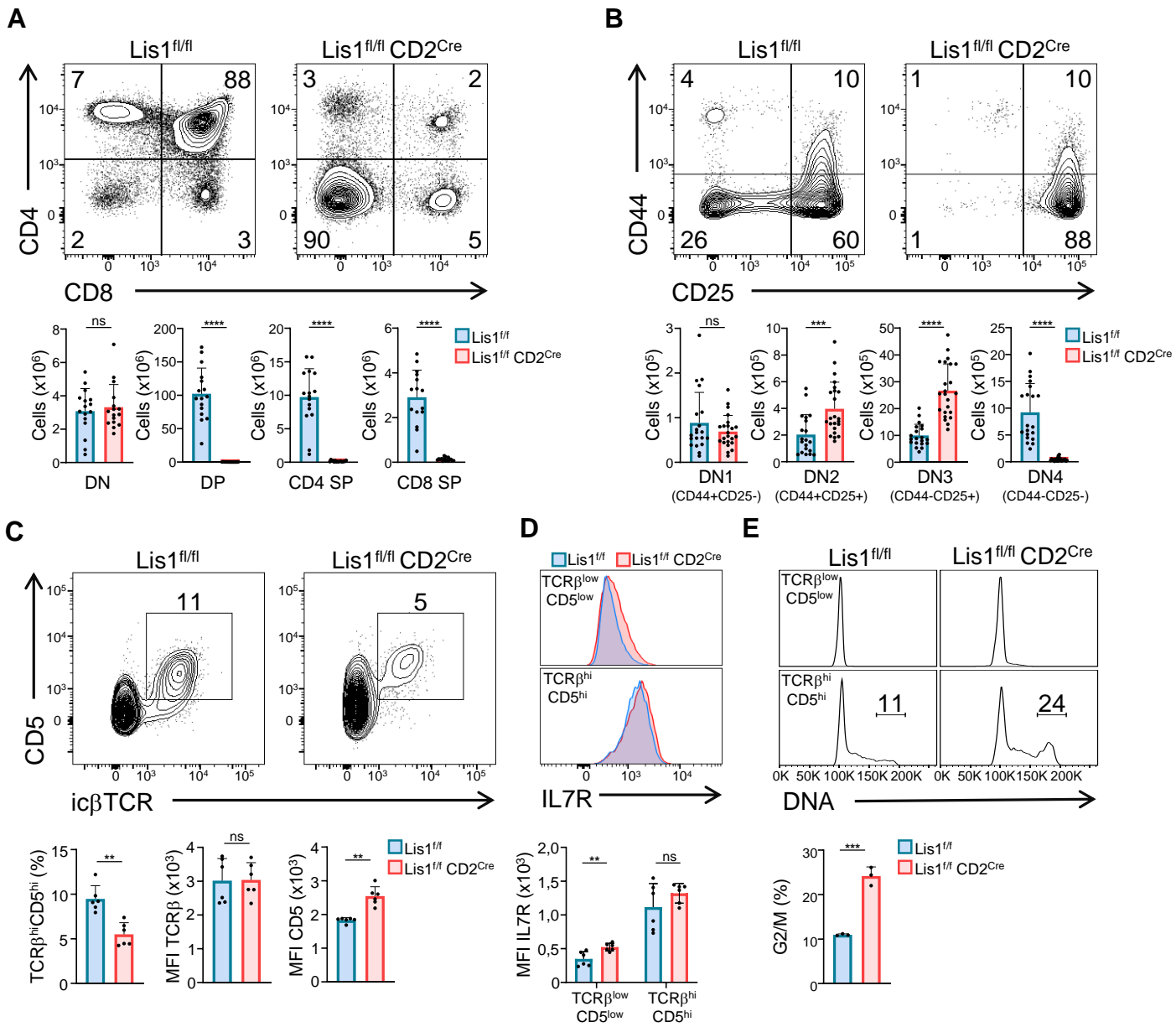


Figure 1 - Figure Supplement 1

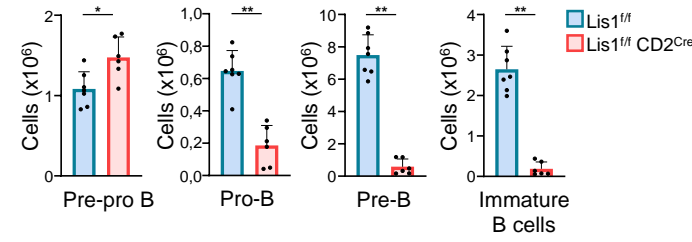
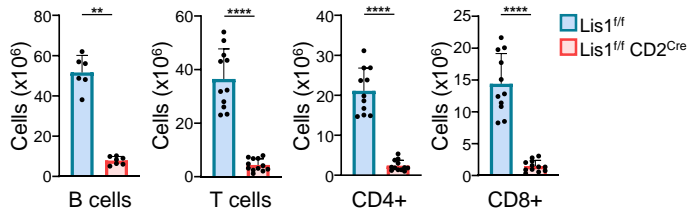
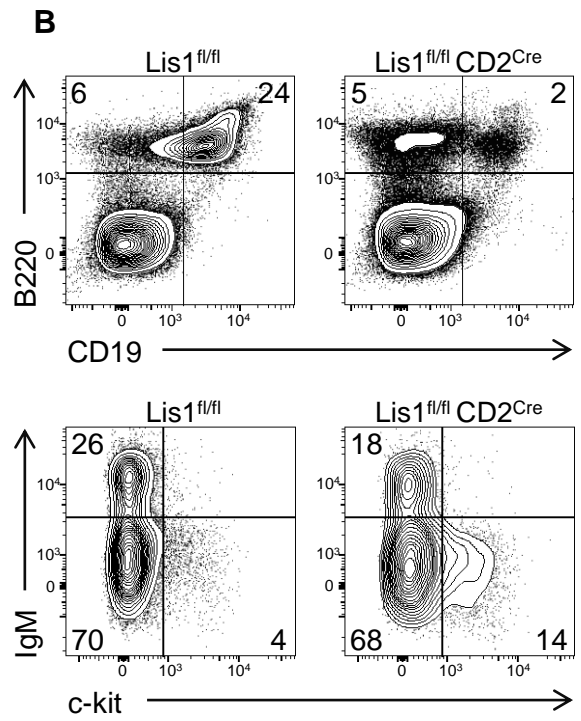
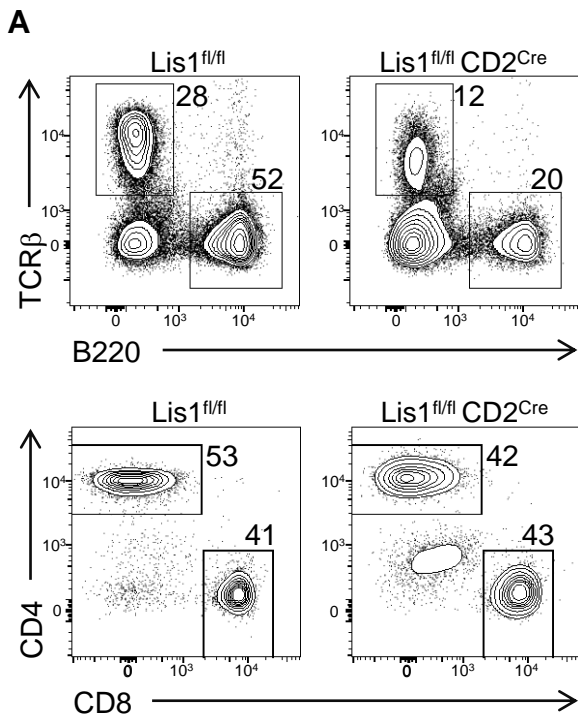


Figure 2

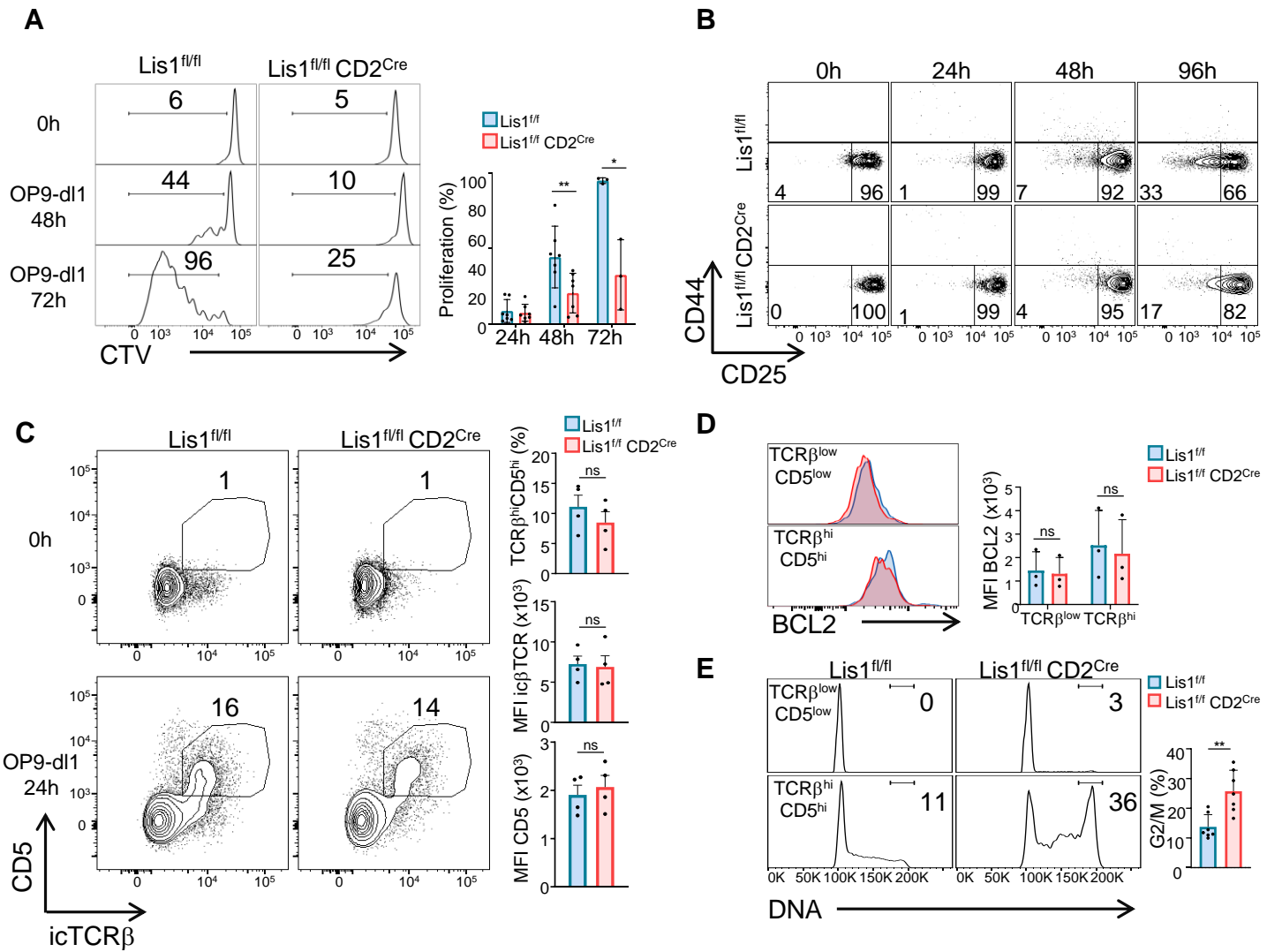


Figure 3 - Figure Supplement 1

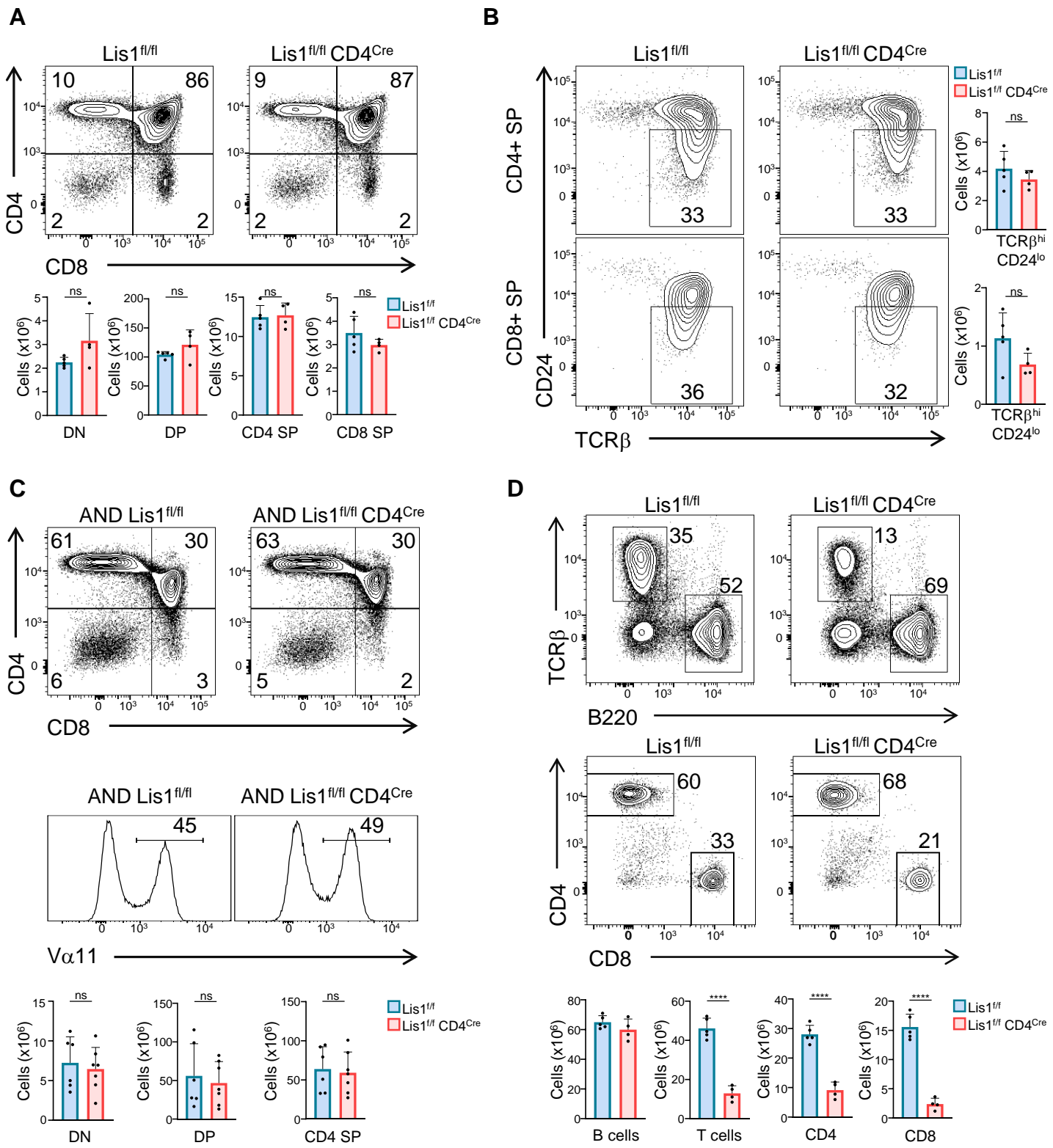


Figure 3

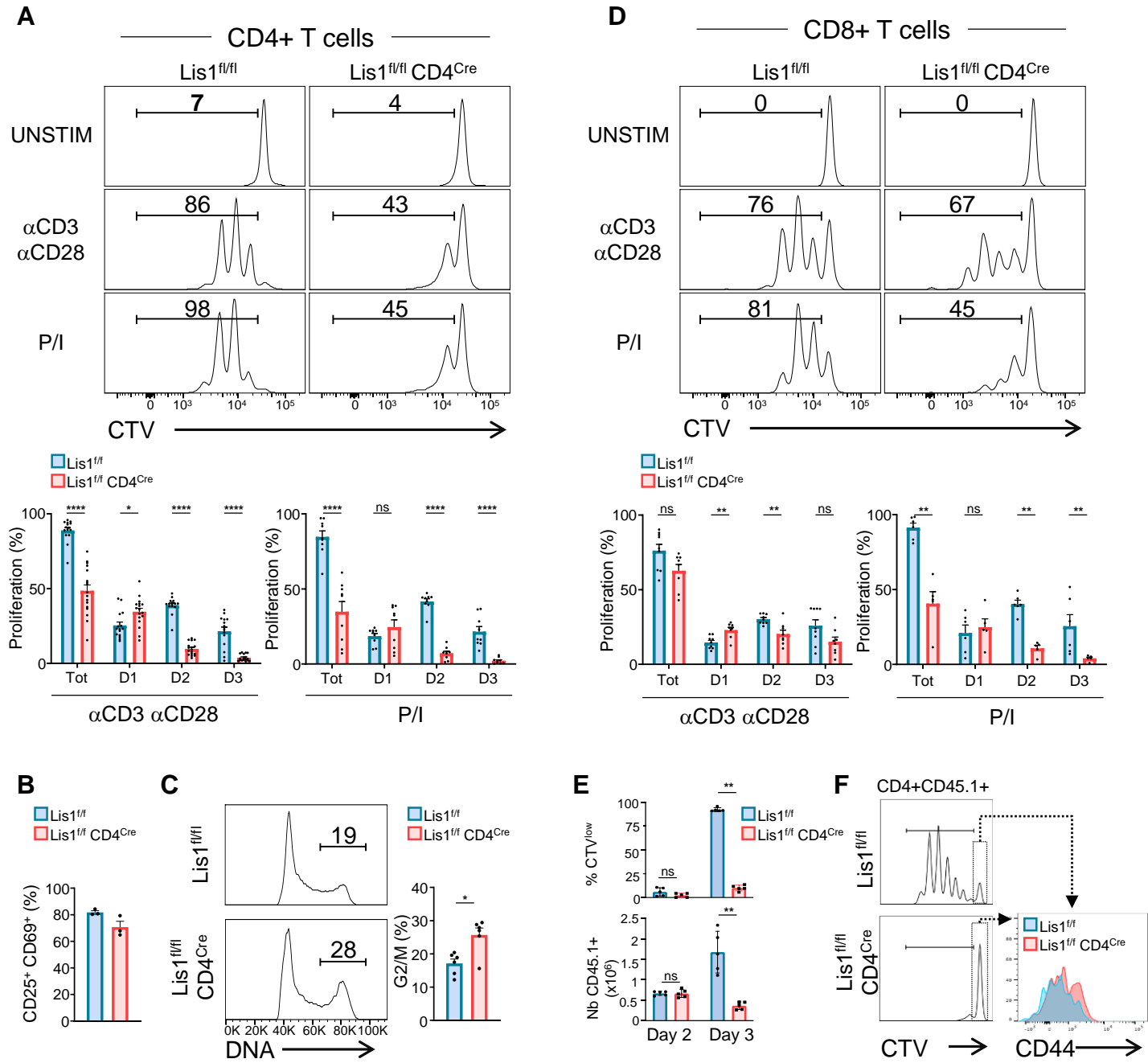


Figure 4

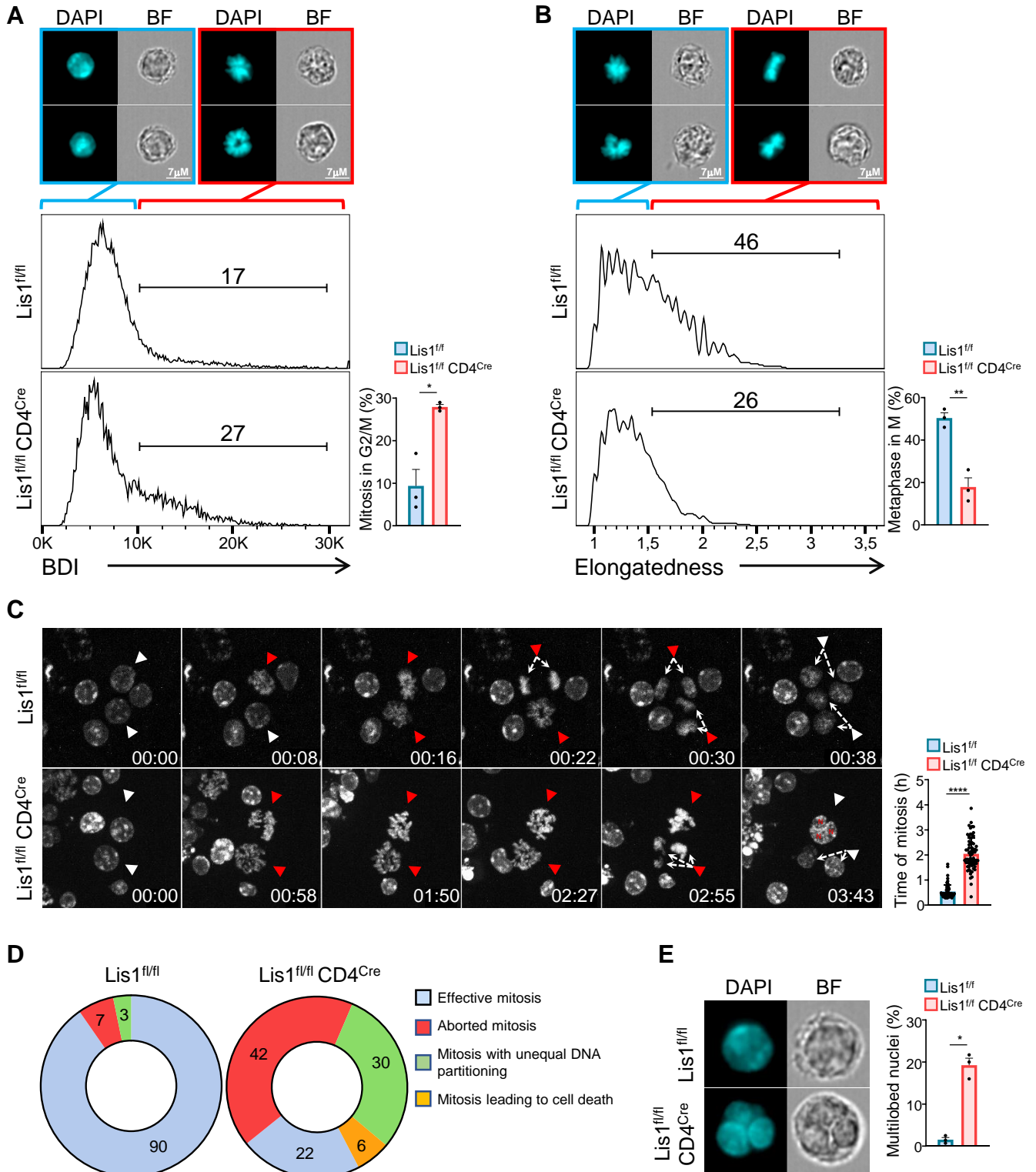


Figure 5

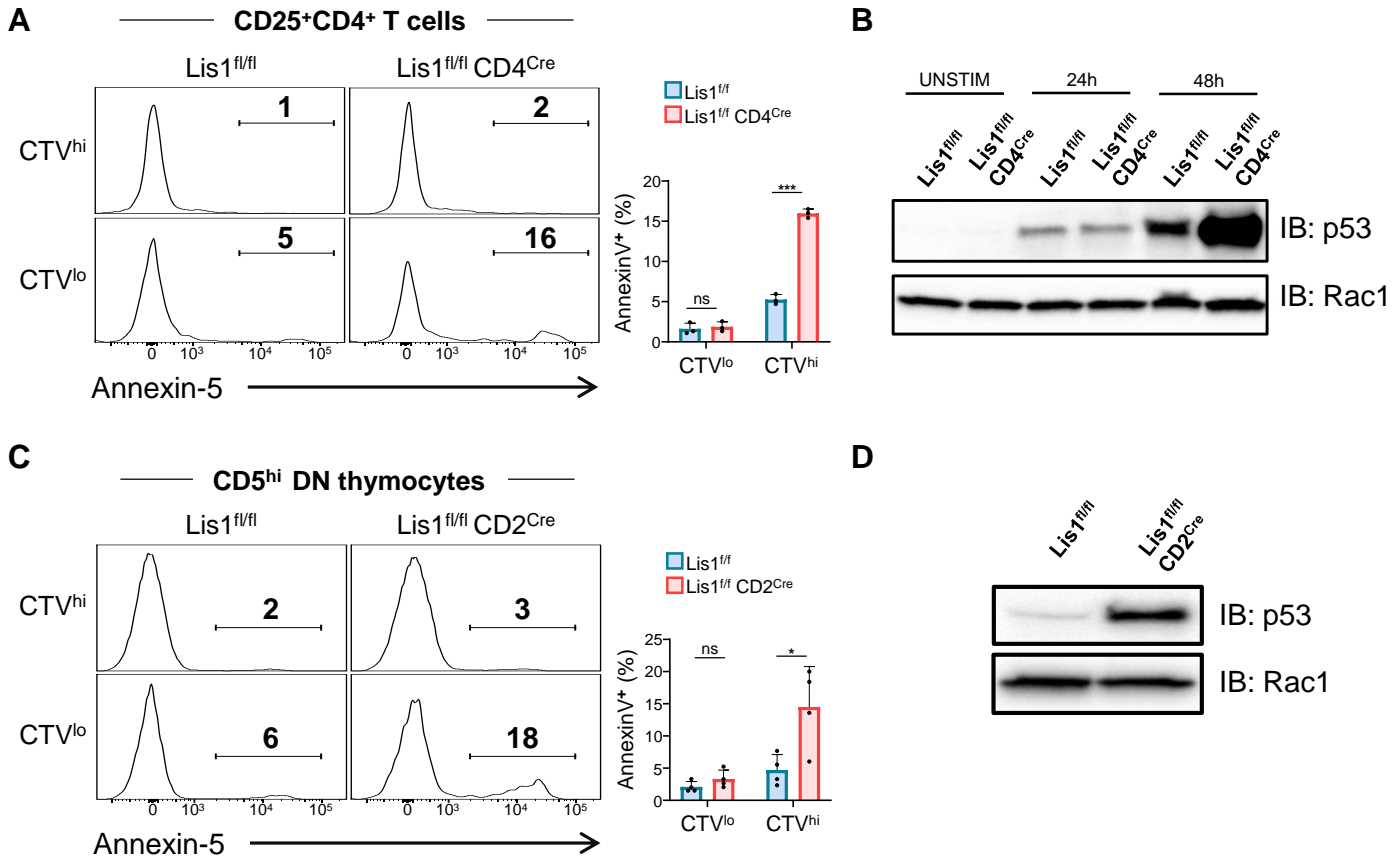


Figure 6

